DEVELOPMENTAL NEUROSCIENCE

Usp11 controls cortical neurogenesis and neuronal migration through Sox11 stabilization

Shang-Yin Chiang[1,2], Hsin-Chieh Wu[1], Shu-Yu Lin[1], Hsin-Yi Chen[3], Chia-Fang Wang[4], Nai-Hsing Yeh[5], Jou-Ho Shih[5], Yi-Shuian Huang[5], Hung-Chih Kuo[4], Shen-Ju Chou[4]*, Ruey-Hwa Chen[1,2]*

The role of protein stabilization in cortical development remains poorly understood. A recessive mutation in the *USP11* gene is found in a rare neurodevelopmental disorder with intellectual disability, but its pathogenicity and molecular mechanism are unknown. Here, we show that mouse *Usp11* is expressed highly in embryonic cerebral cortex, and *Usp11* deficiency impairs layer 6 neuron production, delays late-born neuronal migration, and disturbs cognition and anxiety behaviors. Mechanistically, these functions are mediated by a previously unidentified Usp11 substrate, Sox11. Usp11 ablation compromises Sox11 protein accumulation in the developing cortex, despite the induction of *Sox11* mRNA. The disease-associated Usp11 mutant fails to stabilize Sox11 and is unable to support cortical neurogenesis and neuronal migration. Our findings define a critical function of Usp11 in cortical development and highlight the importance of orchestrating protein stabilization mechanisms into transcription regulatory programs for a robust induction of cell fate determinants during early brain development.

INTRODUCTION

The development of vertebrate cerebral cortex is a dynamic and precisely orchestrated process involving neurogenesis, neuronal migration, and postmigrational cortical organization and circuit formation. In the embryonic mouse cortex, radial glial cells (RGCs) function as neural progenitor cells (NPCs) to give rise to neurons either directly or indirectly via intermediate progenitor cells (IPCs). Newborn neurons migrate along radial fibers in an inside-out manner to form six highly organized layers (*1*). Neurons in each layer exhibit different morphologies, functions, and properties, and even subtle disturbances to neurogenesis or neuronal migration can lead to large defects in the assembly and connectivity of neural circuits. Since cerebral cortex is responsible for higher cognitive functions and emotional processing, malformations of early cortical development could result in a wide range of neurological disorders such as epilepsy, schizophrenia, intellectual disability, and autism (*2*, *3*).

Not unexpectedly, the orderly process of neurogenesis and neuronal migration requires intricate and precise regulation. Previous studies have revealed a complex network of transcriptional programs mediated by transcription factors and chromatin modifiers that govern the dynamics of cortical neurogenesis (*4*, *5*). In addition to transcription, another way to regulate gene expression is the posttranslational control, with regulators affecting protein stability and degradation. Compared to transcriptional regulation, the role of protein degradation in cortical development is less well understood. Several ubiquitin ligases participate in cortical development by targeting key stem/progenitor factors for degradation. For example, Mib and Huwe1 negatively regulate the Notch pathway to promote RGC differentiation (*6*, *7*). Trim11 promotes Pax6 ubiquitination

and degradation, and a negative feedback loop between Trim11 and Pax6 functions to maintain a balanced level of Pax6 during cortical neurogenesis (*8*). Ubiquitin ligases attach ubiquitin chains to proteins to mark them for degradation, whereas deubiquitinating enzymes (DUBs) counteract these effects by removing ubiquitin from proteins. The roles of DUBs in cortical development have been poorly understood, although several of them, such as Usp7, Usp9x, and Uchl1, have been shown to regulate neuronal differentiation and morphogenesis in vitro (*9*–*11*). In principle, DUBs could work hand-in-glove with transcriptional regulators, by promoting the stabilization of differentiation factors once their expression is induced by transcription factors. This could reinforce progenitor cells' commitment to differentiation, by ensuring an irreversible cell fate transition. To test this hypothesis, it is important to define the role of protein deubiquitination events and their interaction with transcriptional networks to coordinate cortical development.

The SoxC family proteins Sox4 and Sox11 are high mobility group box–containing transcription factors that have multiple roles in cortical development (*12*). At early neurodevelopmental stages, Sox4 and Sox11 are critical for neural precursor survival since double knockout (KO) in mouse leads to massive cell death (*13*). Sox4 and Sox11 induce the expression of an overlapping set of neuronal genes (*14*, *15*), but the two transcription factors seem to have nonredundant functions in cortical neurogenesis (*16*). *Sox11* deficiency impairs the generation of early-born neurons by preventing the differentiation of RGCs without affecting IPCs. Sox4, however, is specifically required for the specification and maintenance of IPCs. These discrete functions are likely a result of their restricted expression patterns and distinct binding partners. In addition, Sox11 is required for the radial migration of late-born neurons by preventing precocious dendritic morphogenesis (*17*). In line with their functions in cortical neurogenesis, the expression of Sox4/11 is tightly controlled during this period. In neural precursor cells, their expression is suppressed by the transcriptional repressor RE1-silencing transcription factor (REST)/neuron restrictive silencing factor (NRSF) (*18*). Sox11 is also negatively regulated by transcription factor Lhx2, and this regulation is implicated in fate specification of deep

[1]Institute of Biological Chemistry, Academia Sinica, Taipei 115, Taiwan. [2]Institute of Biochemical Sciences, College of Life Science, National Taiwan University, Taipei 100, Taiwan. [3]Graduate Institute of Cancer Biology and Drug Discovery, College of Medical Science and Technology, Taipei Medical University, Taipei 110, Taiwan. [4]Institute of Cellular and Organismic Biology, Academia Sinica, Taipei 115, Taiwan. [5]Insititute of Biomedical Sciences, Academia Sinica, Taipei 115, Taiwan.
*Corresponding author. Email: rhchen@gate.sinica.edu.tw (R.-H.C.); schou@gate.sinica.edu.tw (S.-J.C.)

layer neurons (*19*). Whether Sox11 can be regulated by a transcription-independent mechanism during cortical development is currently unknown.

USP11, a USP-family DUB, is highly expressed in human brain and exerts an inhibitory role in the self-renewal of glioblastoma stem/initiating cells (*20*). Homozygous missense mutation of the *USP11* gene has been found in a hereditary neurologic disorder patient, characterized by intellectual disability and multiple brain malformations, such as syntelencephaly and corpus callosum agenesis (*21*). However, the pathogenicity of this mutation remains elusive. Here, we show that Usp11 is highly expressed in the developing mouse cortex. Usp11 promotes layer 6 neurogenesis and late-born neuronal migration, and *Usp11* deficiency leads to behavioral abnormalities. Mechanistically, we show that Usp11 deubiquitinates Sox11, which is critical for Sox11 stabilization during cortical development. We provide evidence that the mouse counterpart of human neuro-developmental disorder–associated USP11 variant is defective in Sox11 stabilization and cortical development. Together, our findings reveal an integration of a protein deubiquitination event with a transcriptional network to control cortical development and provide mechanistic insights for how *USP11* mutations cause a human neurological disorder.

RESULTS

Usp11 is highly expressed in mouse embryonic brain including cerebral cortex
Our previous study revealed that *USP11* mRNA is highly expressed in human brain, especially in the forebrain (*20*). This finding prompted us to explore the expression pattern of *Usp11* in mouse. Using whole-mount in situ hybridization, we found that *Usp11* mRNA expression at embryonic day 13.5 (E13.5) is high in the spinal cord and several brain regions, including neocortex (Fig. 1A). Within the cortex, Usp11 is expressed in both neurons (located in preplate and cortical plate) and NPCs (located in ventricular and subventricular zones) during the period of cortical neurogenesis, but the level is higher in neurons than in NPCs (Fig. 1B). These findings imply an up-regulation of Usp11 during neuronal differentiation. Since our previous study found that human *USP11* transcription is repressed by the Notch pathway (*20*), the up-regulation of Usp11 is likely a consequence of Notch inactivation upon the induction of neuronal differentiation. In line with this notion, we showed that mouse *Usp11* was repressed by the Notch/Hes1 axis, as overexpression of an active form of Notch (Notch intracellular domain, referred to as NIC) or Hes1 in a neuroblastoma cell line N2a diminished Usp11 expression and the promoter activity of *Usp11* gene (fig. S1, A and B). Thus, our data suggest a role of Usp11 in cortical neurogenesis.

Usp11 deficiency reduces cortex thickness
To analyze the function of Usp11 in brain development, we obtained a *Usp11* KO mouse from the European Mouse Mutant Archive (EMMA) Mouse Repository (www.infrafrontier.eu/search). This strain harbors a deletion of exons 3 to 10 of the *Usp11* gene (Fig. 1C, top), leading to frameshift and translation stop at exon 11. We performed immunoblot analysis of lysate taken from *Usp11* KO cortices to confirm the absence of Usp11 expression (Fig. 1C, bottom). *Usp11* deletion did not significantly affect body weight and brain weight and only modestly reduced the brain width at postnatal day 7 (P7) (fig. S1, C to F). However, close examination identified a significant reduction of cortex thickness in the *Usp11* KO mice at P7 (Fig. 1, D and E). We

stained for layer-specific markers (Tbr1, Ctip2, and Cux1 for layers 6, 5, and 2 to 4, respectively) and found that *Usp11* deletion did not alter the relative position of cortical layers. However, the thickness of layer 6 and the number of layer 6 neurons were reduced in *Usp11* KO animals, whereas other layers were not significantly affected (Fig. 1, F to H). These findings support a role of Usp11 in regulating the generation of deep layer neurons during cortical development.

Usp11 deficiency impairs the generation of layer 6 neurons
Next, we investigated the role of Usp11 in NPC differentiation into deep layer neurons. Immunostaining for RGC marker Pax6 and IPC marker Tbr2 revealed no significant difference in their gross numbers between wild-type and *Usp11* KO embryos throughout early neurogenesis from E12.5 to E15.5 (fig. S1, G to J). To investigate the reason for fewer Tbr1^{+} layer 6 neurons in the *Usp11* KO cortices, we examined the ratio of cells that exit the cell cycle during early embryonic neurogenesis. We labeled proliferating cells by a pulse of 5-ethynyl-2′-deoxyuridine (EdU) and collected the embryos 24 hours later. We then used Ki67 staining to detect proliferating progenitors when the cortex was collected. Cells labeled by EdU, but not Ki67, are the progenitors that have exited the cell cycle. We observed that *Usp11*-deficient NPCs showed a decreased tendency to exit the cell cycle at E12.5 (Fig. 2, A and B). Since most of the layer 6 neurons are generated from NPCs born at E12.5 (*22*), this finding is consistent with the observation of fewer layer 6 neurons generated in *Usp11* KO. No difference was observed at other time points, consistent with the fact that layers 2 to 5 were not significantly affected in *Usp11* KO. We thus focused on the time point of E12.5 for the following studies. To determine the underlying mechanism for the decreased tendency of cell cycle exit observed in *Usp11* KO NPCs, we performed EdU–5-bromo-2′-deoxyuridine (BrdU) double labeling assay for measuring cell cycle length (*23*). Our data indicated that the *Usp11* deficiency increased cell cycle length of NPCs at E12.5 (Fig. 2C). Furthermore, we did not observe significant differences in cell apoptosis in wild-type and *Usp11* KO cortices during the period of E12.5 to E18.5 (fig. S1, K and L). Thus, our findings uncover a role of Usp11 in regulating NPC cell cycle and the dynamics of NPC differentiation, with the most obvious effect observed from NPCs at E12.5.

To investigate what kinds of cortical progenitor subtypes are affected by Usp11 ablation, we stained Pax6 for RGC and Tbr2 for IPC 1 day after EdU labeling at E12.5 and observed that there were more EdU/Pax6 double-positive cells in *Usp11* KO embryos, compared to control embryos (Fig. 2, D and E). In contrast, *Usp11* deletion did not significantly affect the IPC population (Fig. 2, F and G). These data suggest that *Usp11* deficiency specifically delays RGC cell cycle exit at E12.5, which influences their differentiation into layer 6 neurons. To substantiate this idea, we monitored the generation and distribution of neurons derived from EdU-labeled E12.5 NPCs at E15.5. *Usp11* deletion resulted in a significant reduction in the proportion of Tbr1^{+}EdU^{+} cells and in the distribution of EdU^{+} cells to the cortical plate (Fig. 3, A to C) but did not affect the percentage of Ctip2^{+}EdU^{+} cells (fig. S1, M and N). Since the generation of deep layer neurons is completed at E15.5 (*22*), we also monitored the total Tbr1^{+} cells in E15.5 cortices. Our result indicates that the total Tbr1^{+} cells were diminished in *Usp11* KO compared to wild-type littermates (Fig. 3D). Together, these data are consistent with the findings from gross analysis of the *Usp11* KO cortices at P7 and support a role of Usp11 in RGC differentiation into layer 6 neurons.
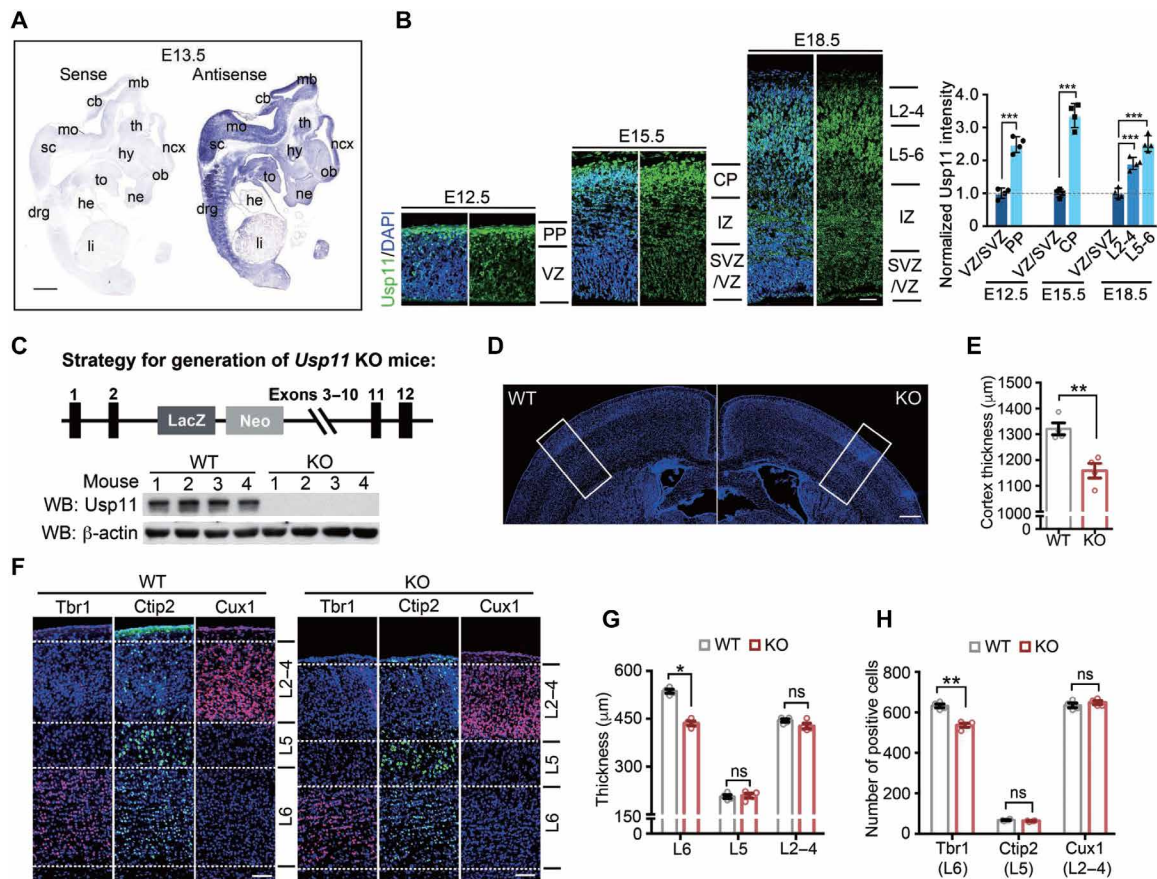
Fig. 1. Usp11 is expressed highly in developing mouse cortex and is important for the generation of layer 6 neurons. (**A**) Whole-mount in situ hybridization analysis of E13.5 mouse embryos using sense or antisense probe of *Usp11*. Scale bar, 500 μm. cb, cerebellum; drg, dorsal root ganglia; he, heart; hy, hypothalamus; li, liver; mb, midbrain; mo, medulla oblongata; ncx, neocortex; ne, nasal epithelium; ob, olfactory bulb; sc, spinal cord; th, thalamus; to, tongue. (**B**) Immunofluorescence analysis for Usp11 expression in the coronal sections of mouse cortices at indicated developmental stages. Scale bar, 100 μm. PP; preplate; IZ, intermediate zone, VZ, ventricular zone; SVZ, subventricular zone; CP, cortical plate. The quantitative data of Usp11 staining intensity (normalized to the intensity in VZ/SVZ at each time point) are shown on the right. (**C**) *Usp11* KO mouse. Top: Schematic presentation of the genomic structure of *Usp11* KO mouse. Bottom: Western blot (WB) analysis of Usp11 expression in the cortices of P7 wild-type (WT) and *Usp11* KO mice. Data of four mice of each genotype are shown. (**D** and **E**) DAPI staining of cortical sections (D) and quantification of cortex thickness (E) of P7 WT or *Usp11* KO mice. Boxes indicate the regions used for quantification. Scale bar, 500 μm. (**F**) Immunostaining for layer-specific markers and DAPI staining on P7 WT or *Usp11* KO cortical sections. Scale bar, 100 μm. (**G** and **H**) Quantitative data for the thickness of indicated cortical layers (G) and number of neurons expressing indicated markers (H) in P7 wild-type or *Usp11* KO cortices. Data in (B), (E), (G), and (H) are means ± SD; *$P < 0.05$, **$P < 0.01$, and ***$P < 0.001$ by *t* test, $n = 4$; ns, not significant.

Usp11 acts in progenitor cells to promote layer 6 neurogenesis

To define whether the role of Usp11 in layer 6 neurogenesis is derived from its direct action in RGCs, we generated *Usp11* floxed mice using CRISPR technology (fig. S2A). We then bred *Usp11* floxed mice with *Emx1*-Cre transgenic line (*24*) to generate *Emx1:Usp11^{f/f}* or *Empty Spiracles Homeobox 1 (Emx1):Usp11^{f/y}* mice (collectively referred to as *Usp11* E-cKO), in which *Usp11* deletion occurs in Emx1-expressing cortical progenitors. In addition, we deleted *Usp11* specifically in the postmitotic neurons by breeding *Usp11* floxed mice with *Nex*-Cre (*25*) to generate *Nex:Usp11^{f/y}* and *Nex:Usp11^{f/f}* mice (collectively referred to as *Usp11* N-cKO) (fig. S2, A and B). Immunofluorescence staining revealed that Usp11 staining intensities in cortical progenitors and neurons were reduced to background levels in *Usp11* E-cKO cortices (fig. S2C). For *Usp11* N-cKO, Usp11 expression remained in the cortical progenitors but was virtually lost in cortical neurons

(fig. S2D). We found that the cortices of *Usp11* E-cKO mice at P7 were thinner than the control mice, with a specific reduction in the thickness of layer 6, but not other layers (fig. S2, E to G). Consistently, the number of Tbr1^{+} (layer 6) neurons was reduced in *Usp11* E-cKO cortices at P7, whereas Ctip2^{+} (layer 5) and Cux1^{+} neurons (layers 2 to 4) were not affected (fig. S2H). However, the cortex thickness and layer 6 thickness did not differ between control and *Usp11* N-cKO mice (fig. S2, I to K), indicating that the defects seen in *Usp11* E-cKO resulted from *Usp11* ablation in cortical progenitors.

In line with this idea, we found that *Usp11* E-cKO increased the number of E12.5-born progenitor cells retained in the RGC state at E13.5 (Fig. 3, E and F). Consistently, the total number of Tbr1^{+} neurons was decreased in the cortices of E15.5 *Usp11* E-cKO mice, compared to the control littermates (Fig. 3G). *Usp11* E-cKO mice at E15.5 also exhibited reductions in the number of layer 6 neurons derived from E12.5-born progenitors and the number of E12.5-born cells
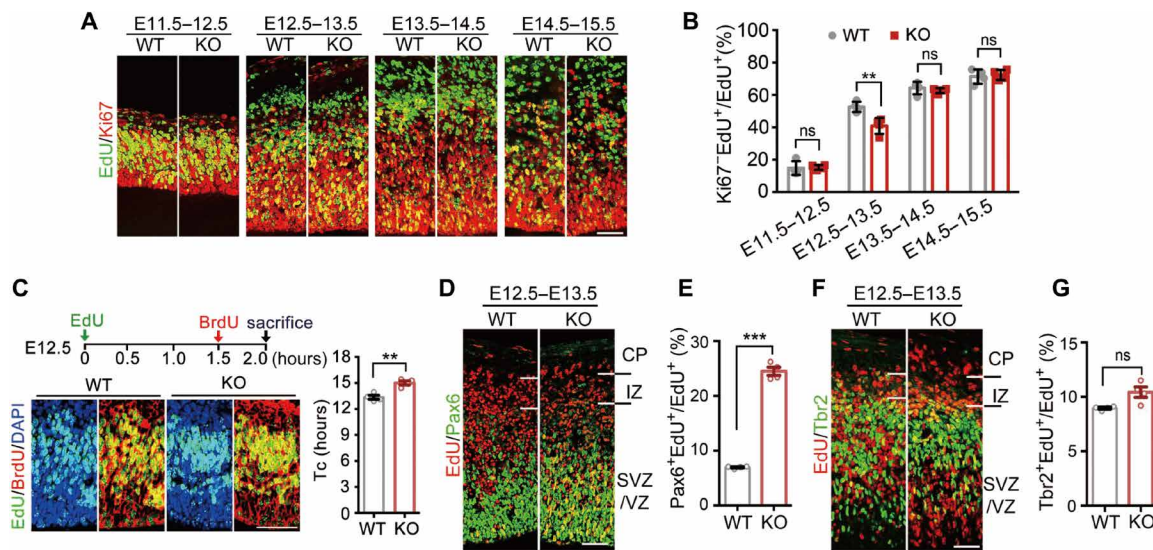
Fig. 2. USP11 regulates RGC cell cycle and proliferation. (**A** and **B**) Immunostaining for EdU and Ki67 (A) and quantitative data (B) for examining NPC cell cycle exit in WT and *Usp11* KO cortices labeled with EdU at each day from E11.5 to E14.5 and harvested 1 day later. Scale bar, 100 μm. (**C**) Top: Schematic diagram of the timing of EdU and BrdU injections and sacrifice to determine the cell cycle length. Bottom panels: Immunostaining for EdU and BrdU and DAPI staining on coronal sections of WT or *Usp11* KO cortices (left) and quantitative data for cell cycle length (right). Scale bar, 100 μm. Method for calculating cell cycle length was described in Materials and Methods. (**D** and **F**) Immunostaining for EdU and Pax6 or Tbr2 on coronal sections of E13.5 WT or *Usp11* KO cortices. EdU was injected at E12.5. Scale bar, 100 μm. (**E** and **G**) Quantification of results from (D) and (F), respectively, showing the percentage of EdU-labeled cells expressing indicated markers. Data in (B), (C), (E), and (G) are means ± SD; **P < 0.01 and ***P < 0.001, by *t* test, *n* = 4.

distributed to the cortical plate (Fig. 3, H to J). These findings provide evidence that Usp11 acts directly in neural progenitors to promote the generation of layer 6 neurons.

### *Usp11* deficiency impairs radial migration of cortical neurons

In *Usp11* KO and *Usp11* E-cKO cortices, we observed a reduction of E12.5-labeled cells to arrive at cortical plates at E15.5 (Fig. 3, C to J). Although these findings are consistent with a differentiation defect of E12.5-born progenitors caused by Usp11 deficiency, Usp11 may elicit an additional effect to directly regulate the radial migration of cortical neurons. To more specifically evaluate the role of Usp11 in the migration of cortical neurons, we thought to focus on the late-born neurons, as the finding that *Usp11* KO did not affect the thickness of the superficial layer (layers 2 to 4) at P7 suggests its dispensable role in the neurogenesis of superficial layers. To substantiate this hypothesis, we performed EdU injection at E15.5, since cortical progenitors at this time point mainly give rise to layers 2 to 4 neurons (*22*). We harvested embryos at E18.5 and analyzed the fate of EdU+ cells by staining for Pax6, Tbr2, or Satb2 (a marker of layers 2 to 4 neurons). We found that *Usp11* KO mice and wild-type littermates showed no difference in total number of EdU+ cells and the percentages of Pax6+EdU+, Tbr2+EdU+, and Satb2+EdU+ cells (Fig. 4A and fig. S3, A to F), indicating that Usp11 ablation does not affect the differentiation of E15.5-born progenitor cells. However, compared to wild-type cortices, *Usp11* KO cortices showed a higher percentage of EdU+ cells in IZ and a lower percentage in layers 2 to 4 (Fig. 4, A and B). In line with this finding, fewer Satb2+EdU+ neurons in *Usp11* KO cortex migrated to their final destination (layers 2 to 4) (Fig. 4C). By P7, however, most EdU+ cells and virtually all EdU+Cux1+ cells had migrated to the superficial layers in both *Usp11* KO and wild-type animals (fig. S3, G to I). These findings

indicate that late-born neuronal migration was delayed by *Usp11* deletion.

Next, we investigated whether the neuronal migration defect seen in the *Usp11* KO mice is due to a cell-autonomous effect. This is important since the migration of upper layer neurons is dependent on radial fibers and can also be regulated by factors secreted from other cell lineages (*26*). To address this question, we analyzed *Usp11* N-cKO and control embryos. *Usp11* N-cKO cortices showed a similar delay in the migration of late-born neurons to *Usp11* KO (Fig. 4, D to F). Thus, Usp11 has a cell-autonomous role in promoting the radial migration of late-born neurons.

Usp11 KO mice exhibit learning/memory and anxiety abnormalities

The defects in neurogenesis and neuronal migration we observed in *Usp11* KO mice suggest that *Usp11* deficiency could impair neuron number, maturation, and connectivity, which might compromise cortical functions. Therefore, we investigated whether *Usp11* KO causes behavior abnormalities related to neurodevelopmental disorders, such as deficits in cognitive function and anxiety. To assess cognitive function, we used Morris water maze (MWM), contextual fear conditioning (CFC), and novel object recognition (NOR) tests for spatial learning/memory, associative learning/memory, and nonspatial memory, respectively. In MWM, we did not observe differences in performance between wild-type and *Usp11* KO mice with a visible platform, demonstrating that their swimming ability and visual acuity were not impaired (fig. S4A). However, when the platform was hidden from the mice during training, the *Usp11* KO mice exhibited deficits in spatial learning by taking more time to locate the platform at day 2 and day 3 (fig. S4B). After they showed no significant difference at day 4, we tested them for memory retention at day 5 by removing the platform and measuring the amount of
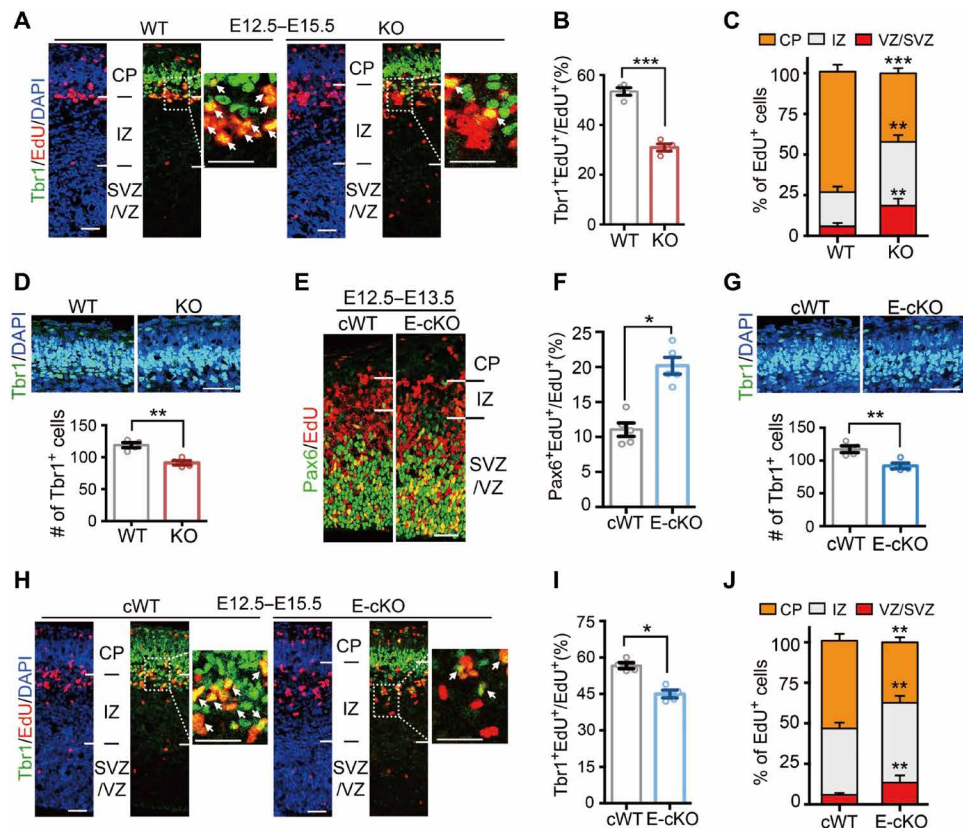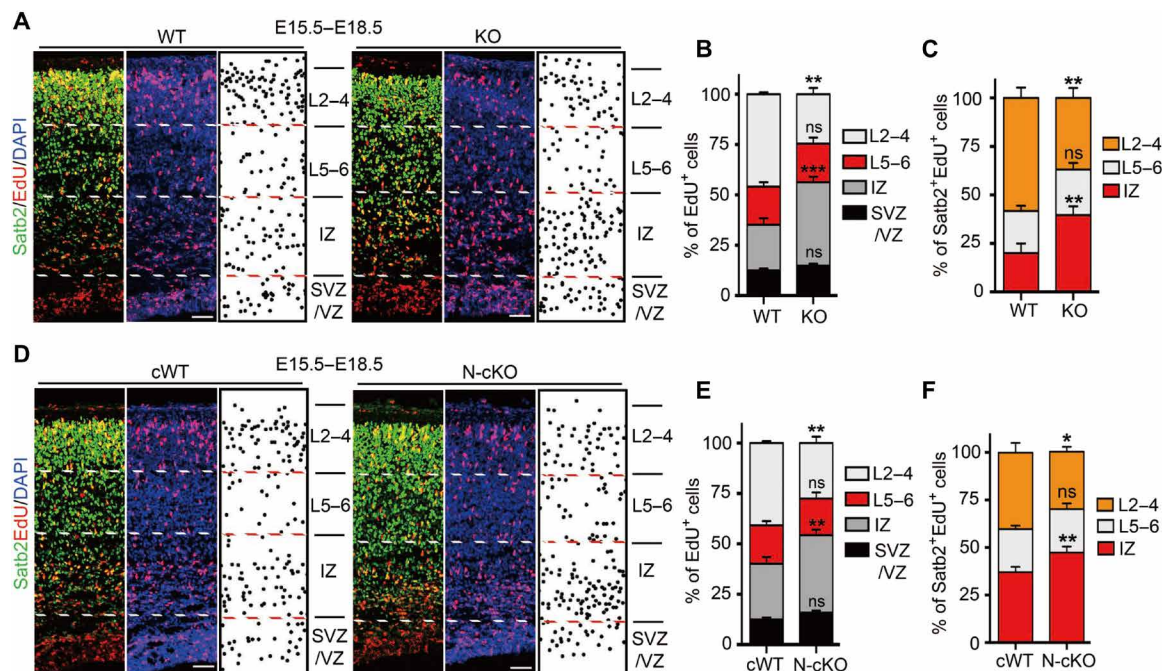
Fig. 3. *Usp11* acts cell-autonomously to promote RGC differentiation. (**A** and **H**) Immunostaining for EdU and Tbr1 on coronal sections of the cortices from E15.5 *Usp11* KO (A) or *Usp11* E-cKO (H) mice and their control littermates. EdU was injected at E12.5. The insets on the right are enlarged images of the area outlined in dotted lines, and arrows mark EdU+ cells expressing Tbr1. Scale bar, 100 μm. (**B** and **I**) Quantification of results from (A) and (H), respectively, showing the percentage of EdU-labeled cells expressing Tbr1. (**C** and **J**) Quantification of results from (A) and (H), respectively, showing the percentage of EdU-labeled cells at indicated locations. (**E**) Immunostaining for EdU and Pax6 on coronal sections of E13.5 control or *Usp11* E-cKO cortices. EdU was injected at E12.5. Scale bar, 100 μm. (**F**) Quantification of results from (E) showing the percentage of EdU-labeled cells expressing Pax6. (**D** and **G**) Immunostaining for EdU and Tbr1 on coronal sections of E15.5 *Usp11* KO (D) or *Usp11* E-cKO (G) mice and their control littermates. Scale bar, 100 μm. Quantification of the total Tbr1+ cells is shown on the bottom. Data in (B), (C), (D), (F), (G), (I), and (J) are means ± SD; *$P < 0.05$, **$P < 0.01$, and ***$P < 0.001$, by *t* test (B, D, F, G, and I) or one-way ANOVA with Tukey's post hoc test (C and J), $n = 4$.

time they spent in the area where the platform was previously located (probe trial). The *Usp11* KO mice spent less time in the target quadrant than wild-type littermates (fig. S4C), indicating a deficit in spatial memory. In the CFC test, mice were trained to express a fear response (freezing) by linking a conditioned stimulus with an aversive unconditioned stimulus (an electronic shock). The wild-type and *Usp11* KO mice did not show differences in habituation and exhibited a similar increase in freezing during the training period at day 1 (fig. S4D, left). While exposed to the context stimulus alone at day 2, they were initially indistinguishable, suggesting no difference in memory retention. However, *Usp11* KO mice showed a slower decline in freezing than wild-type littermates during the extinction tests (fig. S4D, right), suggesting a deficit in memory extinction. Last, in the NOR test, the two groups of mice showed no difference in exploring a novel object, suggesting normal nonspatial memory (fig. S4E). However, when we used the elevated plus maze (EPM) and open field tests to assess anxiety-related behaviors, the *Usp11* KO mice showed increased duration and distance in the open arms of EPM and the center zone of the open field compared to wild-type littermates (fig. S4, F and G), suggesting anxiety and/or attention deficit. Of note, the two groups of mice displayed comparable veloc-

ity (fig. S4G), meaning no differences in their motor activity. Likewise, they performed similarly in the rotarod test (fig. S4H). Together, *Usp11* KO disrupts learning, memory, and anxiety behaviors, consistent with defects in cortical development.

Sox11 is identified as a Usp11 substrate

Having demonstrated the effects of Usp11 deficiency on cortical development, we next sought to define its molecular mechanism. Since *Usp11* encodes a DUB, we reasoned that Usp11 deficiency may lead to increased ubiquitination and degradation of a protein that is critical for neuronal differentiation and migration. We first performed a label-free quantitative liquid chromatography–tandem mass spectrometry (LC-MS/MS) analysis to detect the protein expression profiles in E17.5 wild-type and *Usp11* KO cortices and identified 3871 proteins in four biological repeats. Proteins down-regulated in *Usp11* KO were defined with the following criteria: wild type/*Usp11* KO ratio >1.5, $P < 0.05$, and a total of 122 proteins were recovered (Fig. 5A and table S1). Gene Ontology (GO) analysis with these 122 proteins revealed that neurogenesis and nervous system development are among the enriched terms (fig. S5A), and 7 proteins were found in these two categories (Fig. 5A, marked in red). Since a direct target

Fig. 4. *Usp11* acts cell-autonomously to promote late-born neuronal migration. (**A** and **D**) Immunostaining for EdU and Satb2 on coronal sections of E18.5 WT and *Usp11* KO (A) or cWT and *Usp11* N-cKO (D) cortices. EdU was injected at E15.5. Scale bar, 100 μm. Locations of EdU⁺ cells are depicted to the right. (**B**, **C**, **E**, and **F**) Quantification of results from (A) or (D) showing the percentage of EdU⁺ (B and E) and EdU⁺Satb2⁺ cells (C and F) at each position. Data are means ± SD; *$P < 0.05$, **$P < 0.01$, and ***$P < 0.001$ by one-way ANOVA with Tukey's post hoc test, $n = 4$.

of Usp11 should exhibit not only a decreased protein level but also an increased ubiquitination level in response to Usp11 ablation, we sought to conduct a ubiquitylome analysis to globally assess ubiquitination changes by Usp11. To obtain enough cells for analysis, we used NPCs/neurons induced from mouse embryonic stem (ES) cells via an established protocol (fig. S5B). Neuron formation started at day 8, and *Usp11* up-regulation increased the number of cells expressing the neuron marker Tuj1 (fig. S5, C and D), indicating the ability of this ex vivo model to recapitulate the in vivo neurogenesis-promoting activity of Usp11. We performed an MS-based protocol for ubiquitylome changes (*27*) on day 8 culture with some modifications (fig. S5E). For ubiquitylome analysis, trypsin-digested proteins from cell lysates were subjected to immunoprecipitation with a K-ε-GG antibody, which recognizes the di-glycine remnants of ubiquitinated lysine. Peptides before and after enrichment (for proteome and ubiquitylome analyses, respectively) were labeled with isotopically distinct tandem mass tags (TMTs), thus enabling the quantification of relative abundances of each peptide across samples (*28*). To increase the number of identified peptides, peptides for proteome analysis were fractionated before LC-MS/MS analysis. Among the 1004 proteins uncovered from both proteome and ubiquitylome analyses, 29 displayed [protein-normalized K-ε-GG peptide changes] (Control/Usp11) >1.5 and were thus considered as candidate Usp11 substrates (table S2). Among these 29 proteins, Sox11 is the only protein that was also recovered from the proteome analysis for proteins down-regulated in *Usp11* KO cortices (Fig. 5B and fig. S5F). The proteome analysis also revealed that a number of previously identified Sox11 targets (*14*) were down-regulated by *Usp11* ablation (Fig. 5A, marked in blue). Both Usp11 and Sox11 are nuclear proteins. Furthermore, the phenotypes of *Sox11* deletion in cortical development (*16*, *17*) resemble that of *Usp11* deletion. All of

these observations support Sox11 as a target and effector of Usp11. Consistently with this notion, overexpression of Usp11, but not a catalytically dead mutant, decreased Sox11 ubiquitination levels, whereas Usp11 knockdown resulted in increased Sox11 ubiquitination (Fig. 5, C and D). Using an antibody specific for K48-linked ubiquitin chains, we confirmed that Usp11 expression reduced Sox11 K48-linked polyubiquitination (fig. S6A). Purified Usp11 was capable of directly deubiquitinating Sox11 in vitro (Fig. 5E) and, last, Flag-Sox11 or endogenous Sox11 associated in a complex with endogenous Usp11 in 293T cells, N2a cells, and cells taken from developing mouse cortex (Fig. 5, F and G, and fig. S6B). Together, these data provide evidence that Sox11 is a substrate of Usp11.

Usp11 stabilizes Sox11 during cortical neurogenesis

We next analyzed the functional consequence of Sox11 deubiquitination by Usp11. Knockdown of Usp11 in N2a cells using three independent short hairpin–mediated RNAs (shRNAs) markedly reduced Sox11 protein level without affecting its mRNA level (Fig. 6A and fig. S6C). Conversely, overexpression of Usp11, but not a catalytically dead mutant, elevated Sox11 protein abundance (Fig. 6B). Human USP11 also up-regulated SOX11 expression (fig. S6D), demonstrating the evolutional conservation of the Usp11/Sox11 axis. In Usp11 knockdown cells, treatment with the proteasome inhibitor MG132 mitigated the effect of Usp11 knockdown on Sox11 levels (Fig. 6C). Last, using a cycloheximide-chase assay, we found that Usp11 knockdown decreased the stability of Sox11 (Fig. 6D). These data indicate that Usp11 stabilizes Sox11 by preventing its proteasomal degradation.

Sox11 is regulated at the transcriptional level during cortical neurogenesis (*18*). Our identification of an additional level of regulation (i.e., at the protein stability level) by Usp11 prompted us to investigate the kinetics of *Sox11* mRNA level changes and protein level
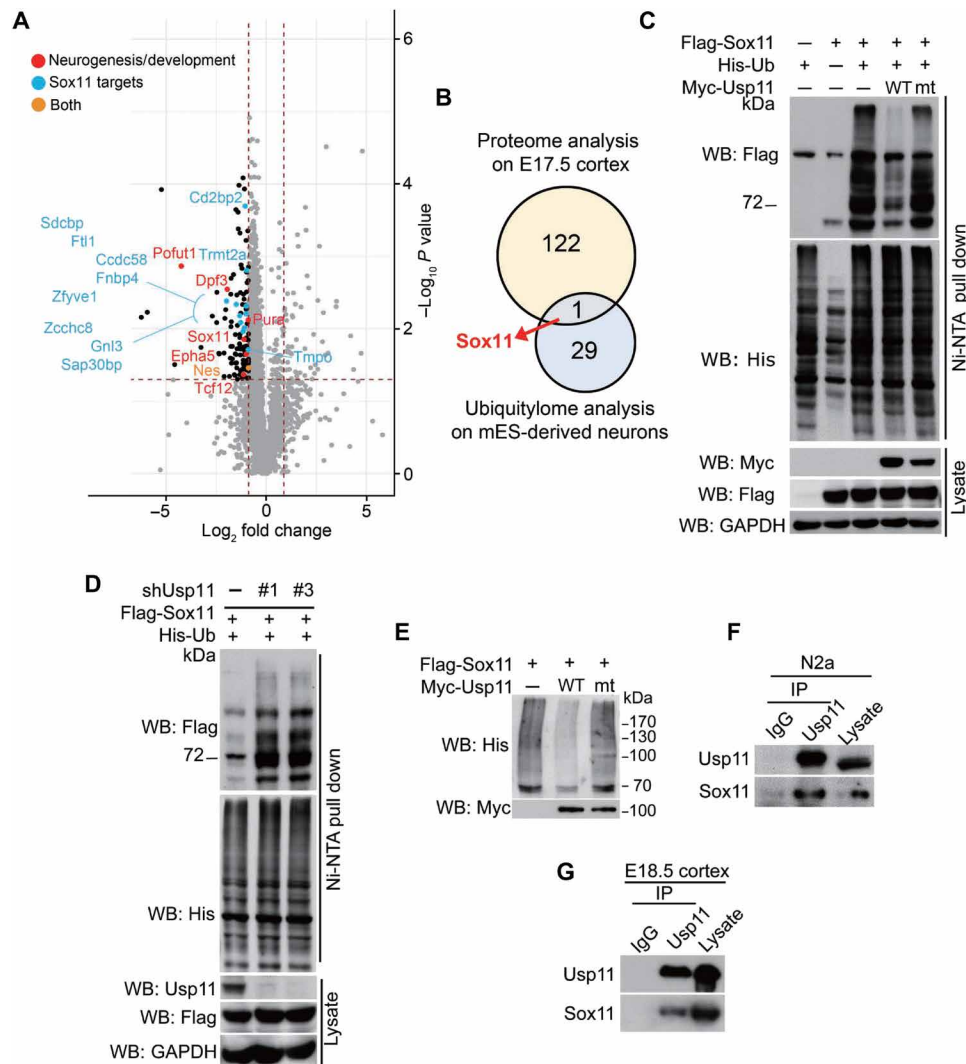
Fig. 5. Usp11 deubiquitinates Sox11. (**A**) The volcano plot of the proteins identified from WT and *Usp11* KO cortices by label-free quantitative LC-MS/MS. The proteins are plotted according to their $\log_2$ fold changes (*x* axis) and $\log_{10}$ *P* values (*y* axis). Proteins down-regulated in *Usp11* KO are shown as black dots. Among them, proteins with known functions in neurogenesis or nervous system development are marked in red, the known targets of Sox11 are in blue, and the protein with both features is in orange. (**B**) Venn diagram of the number of proteins down-regulated in *Usp11* KO cortices uncovered from proteome analysis (four biological replicates) overlapping with that showing a decreased ubiquitination in Usp11 overexpressed neurons identified from ubiquitylome analysis (one biological replicate). (**C** and **D**) Analysis of Sox11 ubiquitination levels in 293T cells transfected with indicated constructs (C) or N2a cells stably expressing indicated shRNAs and transfected with indicated constructs (D). The cellular ubiquitinated proteins were pulled down by Ni-NTA beads under denaturing conditions and then analyzed by Western blot. (**E**) In vitro deubiquitination assay using purified and ubiquitinated Sox11 and separately purified Usp11. (**F** and **G**) Immunoprecipitation analysis of the interaction between endogenous Usp11 and endogenous Sox11 in N2a cells (F) or lysate of mouse cortex (G). IgG, immunoglobulin G.

changes during neurogenesis. We performed ex vivo and in vivo experiments. For the ex vivo experiment, we induced neuronal differentiation of NPCs isolated from E12.5 mouse cortex. Successful neuron induction was confirmed by a gradual increase in *Tuj1* expression and a decrease in *Pax6* expression (Fig. 6E). During this period, *Sox11* mRNA was only modestly elevated (~1.4-fold for day 3 versus day 0). Nevertheless, we found a sevenfold elevation to its protein level (Fig. 6F). Similarly, although *Sox11* mRNA and protein expression in mouse cortex were both elevated during E10.5 to E14.5, the fold induction of protein was higher than mRNA (Fig. 6, G to I). In *Usp11* KO cortices, although *Sox11* mRNA was induced at levels similar to that in wild-type cortices, Sox11 protein induction

was greatly impaired. The Sox11 protein induction folds detected by Western blot seem to be a little higher than that from the proteomics analysis, presumably due to different methods used. Together, our data collectively indicate that the induction of *Sox11* mRNA during cortical neurogenesis is insufficient to lead to a robust protein elevation and that Usp11-dependent Sox11 stabilization accounts for a major role in Sox11 up-regulation during cortical neurogenesis.

Among the Sox family proteins, Sox4 is the most closely related member to Sox11. However, no interaction between Sox4 and Usp11 could be detected using E18.5 cortical lysates (fig. S6E). Consistently, wild-type and *Usp11* KO cortices during E12.5 to E18.5 expressed comparable amounts of Sox4 protein (fig. S6F). In addition, the
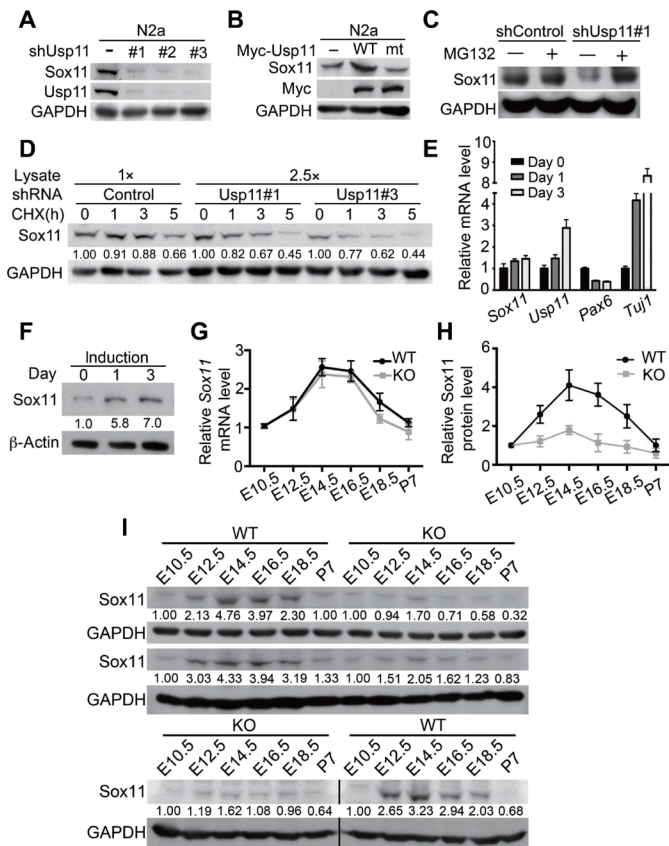
Fig. 6. USP11 stabilizes Sox11 to result in a robust Sox11 induction during cortical development. (**A** and **B**) Western blot analysis of Sox11 expression in N2a cells expressing indicated shRNAs (A) or in 293T cells transfected with indicated constructs (B). (**C** and **D**) Western blot analysis of Sox11 expression in N2a cells stably expressing indicated shRNAs and treated with MG132 for 16 hours (C) or cycloheximide for indicated time points (D). Of note, for an accurate comparison of protein turnover, a higher amount (2.5-fold) of lysates from Usp11 knockdown cells was loaded (D). The levels of Sox11 are normalized to that in 0 hours and indicated on the bottom. (**E** and **F**) RT–quantitative PCR (qPCR) (E) and Western blot (F) analyses of the expression of indicated genes/proteins at indicated time points during neuron induction using NPCs isolated from E12.5 cerebral cortices. The relative amounts of Sox11 are indicated on the bottom (F). (**G**) RT-qPCR analysis of the expression of Sox11 mRNA in the cortices of Usp11 KO or wild-type littermates at indicated developmental stages. (**H** and **I**) Western blot analysis of Sox11 expression in the cortices of Usp11 KO or wild-type littermates at indicated developmental stages. The three repeats of Western blots and quantitative data are shown in (H) and (I), respectively. In (E), (G), and (H), data are means ± SD, n = 3.

expression of Pml, a Usp11 substrate previously identified in brain tumors (20), was comparable in wild-type and Usp11 KO cortices (fig. S6F). Thus, our findings indicate that the function of Usp11 in cortical neurogenesis is unlikely mediated by Sox4 and Pml.

Usp11 stabilization of Sox11 is required for cortical development

To define the contribution of Sox11 stabilization to the effects of Usp11 on cortical development, we performed rescue experiments. In particular, we intended to test whether Sox11 overexpression rescues the phenotypes of Usp11 deficiency. To do so, we first tested whether Usp11 knockdown causes the same cortical developmental defects observed in Usp11 KO, and second, we examined whether

these defects are rescued by Sox11 overexpression. Using in utero electroporation (IUE) to transfect control or Usp11 shRNA expression constructs at E12.5, we found that Usp11 knockdown by two independent shRNAs greatly reduced the number of Tbr1^{+} neurons at E15.5 (Fig. 7, A and B). Consequently, most Usp11 shRNA-expressing cells (marked by mCherry) did not arrive at cortical plates at this time point, in sharp contrast to cells expressing control shRNA (Fig. 7, A and C). Thus, by up-regulating Sox11, we could rescue the defects in early cortical neurogenesis caused by Usp11 knockdown. To analyze the migration of late-born neurons, we performed IUE at E15.5 and analyzed cortices at E18.5. Compared to cells carrying control shRNA, more Usp11 shRNA-expressing cells stayed at IZ and less migrated to cortical plate (Fig. 7, D and E). Furthermore, Usp11 knockdown decreased the arrival of Satb2^{+} neurons to the superficial layers, an indication of a migration defect (Fig. 7F). Sox11 overexpression was sufficient to partially rescue this migration defect of late-born neurons. Together, our findings provide evidence for the contribution of Sox11 stabilization to the functions of Usp11 in cortical development.

Disease-associated Usp11 mutant is defective in Sox11 stabilization and cortical development

A recent study reported the presence of a homozygous USP11 mutation (R241Q) in a patient with malformations of several brain regions and intellectual disability (21). This residue is evolutionarily conserved and located near the ubiquitin-like (UBL) domain (fig. S7), which is implicated in the binding of substrates or modulators (29). To test the potential pathogenicity of this mutation, we investigated its impact on Sox11 regulation. Whereas expression of wild-type Usp11 increased Sox11 abundance, this mutant did not up-regulate Sox11 (Fig. 8A). Accordingly, the Usp11 R241Q mutant failed to reduce Sox11 ubiquitination level when overexpressed in cells (Fig. 8B). Moreover, the R241Q mutant exhibited a reduced ability in binding Sox11 (Fig. 8C). Thus, the disease-associated USP11 mutant is defective in targeting Sox11 for deubiquitination and stabilization.

To assess the in vivo functions of Usp11 R241Q mutant during cortical development, we used IUE experiments to introduce wild-type and Usp11 R241Q in Usp11-depleted conditions. As expected, Usp11 knockdown decreased the expression of Sox11. This Sox11 down-regulation was rescued by re-expression of wild-type Usp11, but not Usp11 R241Q (Fig. 8, D and E). Functionally, while wild-type Usp11 could completely rescue the defects of Usp11 knockdown in generation of Tbr1^{+} neurons and migration of upper layer neurons, the Usp11 R241Q mutant failed to do so (Fig. 9, A to F). These data provide evidence that the disease-associated Usp11 mutant is defective in Sox11 stabilization, neurogenesis, and neuronal migration and support the pathogenicity of this mutation.

DISCUSSION

Using conventional and conditional KO models, we have provided evidence for dual roles of Usp11 in cortical development—promoting the differentiation of RGCs into layer 6 neurons and then the migration of late-born neurons, through a cell-autonomous manner. We show that these effects of Usp11 are mediated in part by Sox11, which was previously shown to contribute to neurogenesis and neuronal migration in the developing cortex (16, 17). Even though Sox11 is transcriptionally up-regulated during cortical development, our findings reveal an additional layer of regulation—protein stability.
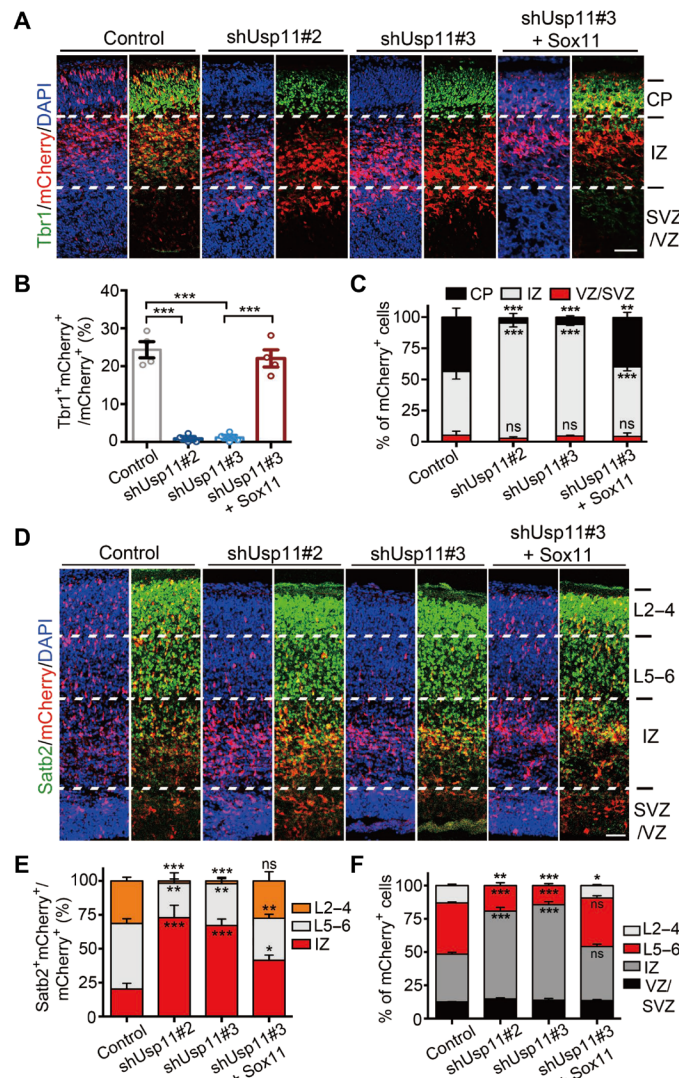
Fig. 7. Sox11 stabilization contributes to the functions of Usp11 in cortical development. (**A**) Immunostaining for Tbr1 and DAPI staining of cortical sections of E15.5 embryos electroporated in utero with indicated constructs and mCherry expressing construct at E12.5. The transfected cells are marked by mCherry. Scale bar, 100 μm. (**B** and **C**) Quantification of results from (A) showing the percentage of transfected cells expressing Tbr1 (B) and the location of transfected cells (C). Data are means ± SD; **$P < 0.01$ and ***$P < 0.001$ by one-way ANOVA with Tukey's post hoc test, $n = 4$. (**D**) Immunostaining for Satb2 and DAPI staining of cortical sections of E18.5 embryos electroporated in utero with indicated constructs and mCherry expressing construct at E15.5. The transfected cells are marked by mCherry. Scale bar, 100 μm. (**E** and **F**) Quantification of results from (D) showing the locations of mCherry+Satb2+ cells (E) and mCherry+ cells (F). Data are means ± SD; *$P < 0.05$, **$P < 0.01$, and ***$P < 0.001$ by one-way ANOVA with Tukey's post hoc test, $n = 4$.

These findings highlight the importance of protein deubiquitination/stabilization for the robust induction of molecular determinants of cell fate and morphogenesis to ensure an irreversible developmental process. We reason that this posttranslational mechanism is particularly needed to extend the half-life of a labile protein, such as Sox11. Notably, since Usp11 is itself regulated at the transcriptional level by Notch signaling, our study indicates that the Usp11-mediated posttranslational regulation of Sox11 is integrated into the transcrip-
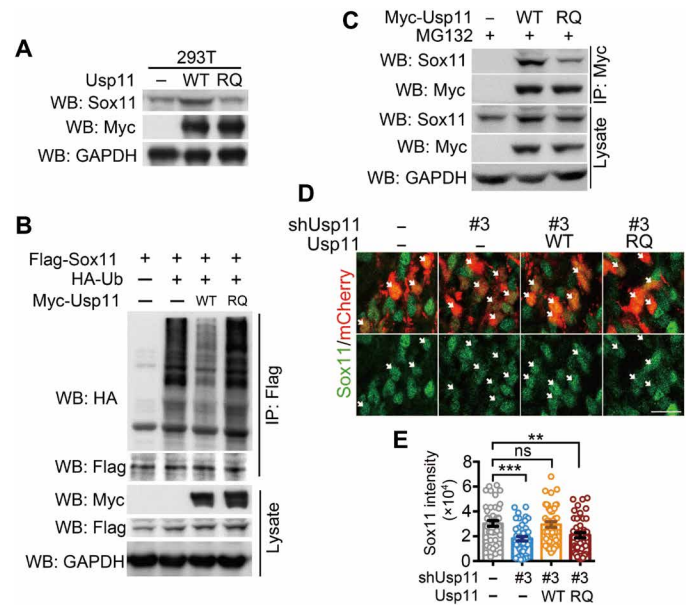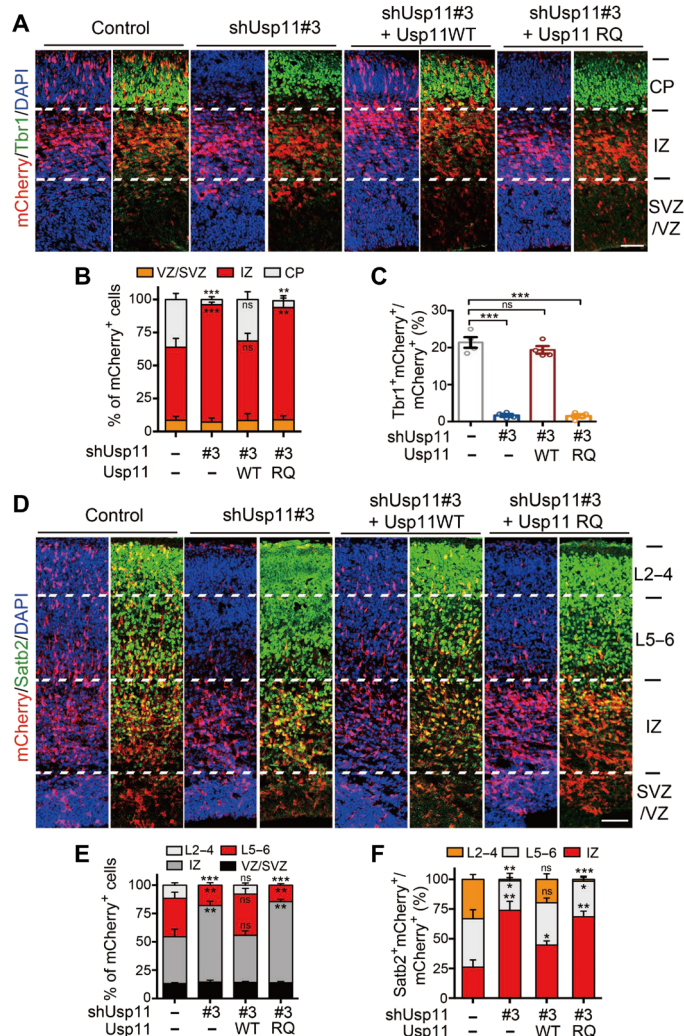

Fig. 8. Disease-associated Usp11 mutant is defective in regulating Sox11. (**A**) Western blot analysis of SOX11 expression in 293T cells expressing Usp11 WT or R241Q mutant. (**B**) Analysis of Sox11 ubiquitination levels in 293T cells transfected with indicated constructs. Sox11 was immunoprecipitated from cell lysates and analyzed by Western blot. (**C**) Immunoprecipitation analysis of the interaction of wild-type or mutant Usp11 with endogenous SOX11 in 293T cells. To prevent SOX11 degradation, the transfected cells were treated with MG132 for 16 hours before harvest. (**D** and **E**) Immunostaining of Sox11 using cortical sections of E15.5 embryos electroporated in utero with indicated shRNA and cDNA constructs and mCherry expressing construct at E12.5. The transfected cells are visualized by mCherry and marked by arrows. Scale bar, 20 μm. The Sox11 immunofluorescence intensities in mCherry+ cells were quantified and shown in (E). Data are means ± SD; **$P < 0.01$ and ***$P < 0.001$ by t test, $n = 45$.

tional circuits governed by Notch and Sox11, thus facilitating the proper development of mouse cortex.

One intriguing question is whether the functions of Usp11 in layer 6 neurogenesis and upper layer neuronal migration are interconnected. On the basis of our findings with *Usp11* N-cKO and *Usp11* E-cKO mice, we believe that they most likely represent separate functions of Usp11 occurring in different cell populations and at different developmental period. While the layer 6 neurogenesis function represents a cell-autonomous action of Usp11 in E12.5-born NPCs, the late-born neuronal migration function is attributed to Usp11's function in the postmitotic neurons.

In addition to the cortical developmental defects observed from *Usp11* KO embryos, adult *Usp11* KO mice exhibited a number of behavior abnormalities, including anxiety and learning/memory deficits. It is currently unclear whether these behavior abnormalities originated from defects in the cerebral cortex development. Nevertheless, impairment of layer 6 neurogenesis has been linked to learning/memory deficit. For instance, sevoflurane exposure of pregnant mice causes layer 6 neurogenesis defect and learning/memory abnormality (*30*). In addition, the layer 6 marker *Tbr1* is essential for specifying layer 6 identity (*31*), and its heterozygous variants have been found in patients with autism spectrum disorder (*32*). Despite these linkages of layer 6 neurogenesis defect to abnormal behaviors, we cannot rule out the possibility that the behavior abnormalities

Fig. 9. Disease-associated Usp11 mutant is defective in supporting cortical neurogenesis and neuronal migration. (**A**) Immunostaining for Tbr1 and DAPI staining using cortical sections of E15.5 embryos subjected to IUE of indicated constructs and mCherry expressing construct at E12.5. The transfected cells are marked by mCherry. Scale bar, 100 μm. (**B** and **C**) Quantification of results from (A) showing the location of transfected cells (B) and the percentage of transfected cells expressing Tbr1 (C). Data are means ± SD; **$P < 0.01$ and ***$P < 0.001$ by one-way ANOVA with Tukey's post hoc test, $n = 4$. (**D**) Immunostaining for Satb2 and DAPI staining using cortical sections of E18.5 embryos electroporated in utero with indicated constructs and mCherry expressing construct at E15.5. The transfected cells are marked by mCherry. Scale bar, 100 μm. (**E** and **F**) Quantification of results from (D) showing the location of mCherry⁺ cells (E) or mCherry⁺Satb2⁺ cells (F). Data are means ± SD, *$P < 0.05$, **$P < 0.01$, and ***$P < 0.001$ by one-way ANOVA with Tukey's post hoc test, $n = 4$.

of *Usp11* KO mice are caused by migration defect of upper layer neurons or an uncharacterized developmental defect in other brain regions.

Notably, the learning/memory deficit seen in *Usp11* KO mice resembles the intellectual disability observed from a neurodevelopmental disorder patient carrying a homozygous missense mutation in the *USP11* gene (*21*). The patient also exhibits malformations of cortical development (MCD) such as syntelencephaly and corpus

callosum agenesis. Since this is the only reported mutation in *USP11* in human disease and because this and other variants are present in publicly available exome and genome databases, we sought to test the functional consequences of this variant. We provide evidence that the mouse counterpart of this USP11 mutant not only is defective in binding and deubiquitinating Sox11, leading to its persistent degradation, but also fails to rescue cortical developmental defects caused by *Usp11* depletion. Thus, by comparing the information gained from the patient with the experimental data derived from this study, including in vivo characterization, behavior tests, and biochemical analyses, we hypothesize that the inability to stabilize Sox11 likely represents a major mechanism for the behavioral and brain architectural abnormalities seen in this patient. Consistent with this hypothesis, heterozygous deletion, truncation, and missense mutations in the *Sox11* gene have been linked to Coffin-Siris syndrome, a congenital disorder characterized by intellectual disability, MCD, and other developmental defects (*33*).

We show that Sox11 overexpression rescues the defects in RGC differentiation and neuronal migration caused by Usp11 deficiency, which supports the contribution of Sox11 stabilization to the effects of Usp11 on cortical development. Nevertheless, we do not exclude the possibility for the involvement of other Usp11 substrates in these functions. Our previous study identified a role of USP11 in the deubiquitination and stabilization of promyelocytic leukemia protein (PML) in glioblastoma (*20*). Notably, *Pml* deficiency leads to an increase in NPC cycling and an impairment of the transition from RGCs to IPCs, thereby resulting in reduced neurogenesis and cortex thickness (*34*). These phenotypes are not entirely consistent with that of *Usp11* deficiency. Accordingly, we could not detect an obvious difference in Pml abundance between wild-type and *Usp11* KO cortices. This finding suggests a context-dependent effect of Usp11 on Pml and a dispensable role of Pml in Usp11's function during cortical development.

It is intriguing that Usp11 targets Sox11, but not its paralog Sox4, in the developing cortex. The inability of Usp11 to regulate Sox4 may be due to an intrinsic difference in the sequences of the two proteins. Notably, although the two proteins share many redundant functions in cortical development (*13, 35, 36*), KO mouse studies have revealed the unique/noncompensatory functions of Sox11 in RGC differentiation in early neurogenesis and migration of late-born neurons (*16, 17*), consistent with the phenotypes of *Usp11* KO mice. Similarly, *SOX11* haploinsufficiency cannot be compensated for by *SOX4* in human and results in neurodevelopmental disorders (*33, 37, 38*). These nonredundant functions could be partly explained by the overlapping but nonidentical expression patterns of the two proteins in developing cortex (*16*). We postulate that the selectivity of Usp11 for Sox11 may result in a specific impairment of layer 6 neurogenesis seen in *Usp11* KO mice. Perhaps Sox11 is uniquely required for the generation of this layer of neurons, while Sox11 and Sox4 are functionally redundant in the neurogenesis of other layers. Accordingly, despite the fact that Usp11 is capable of regulating Sox11 abundance in the cortex during the period of E12.5 to E18.5, *Usp11* ablation elicits a transient effect on NPC differentiation in cerebral cortex, with E12.5-born NPCs showing the most prominent defects. In summary, our study identifies the functions of Usp11-mediated Sox11 stabilization in cortical development, provides an explanation for the association of *Usp11* mutation with neurological disorder, and highlights the importance of deubiquitination-triggered protein stabilization in the developmental process.

MATERIALS AND METHODS

Plasmids

Plasmids encoding human USP11, His-ubiquitin, and myc-NIC were described previously (20). Complementary DNA (cDNA) for mouse *Usp11* was amplified by reverse transcription polymerase chain reaction (RT-PCR) from N2a cells and then subcloned to pRK5-myc and pBybe-myc. *Usp11* C275/283S (CS) and R241Q mutants and human USP11 R241Q mutant were generated by Pfu site-directed mutagenesis (Thermo Fisher Scientific). *Hes1* and *Sox11* cDNAs were purchased from Origene and subcloned to pRK5-Flag and/or pUS2. To clone *Usp11* promoter, a DNA fragment corresponding to nucleotides from −1667 to +343 of the mouse *Usp11* gene was amplified from the genomic DNA of N2a cells and inserted to pGL3-based vector.

Antibodies and reagents

Antibodies used in this study are listed in table S3. Cycloheximide was purchased from Sigma-Aldrich. MG132 was obtained from Calbiochem.

Cell culture and transfection

293T cells were cultured in Dulbecco's modified Eagle's medium (DMEM), supplemented with 10% fetal bovine serum (FBS) and penicillin/streptomycin (PS; 100 U/ml). N2a mouse neuroblastoma cells were maintained in high-glucose minimal essential medium (MEM) supplemented with 10% FBS, 1 mM GlutaMax, and PS (100 U/ml). D3 mouse ES cells were maintained in undifferentiated state on a feeder layer of mitomycin C–inactivated mouse embryonic fibroblasts in ES medium [DMEM supplemented with 15% FBS, 55 μM β-mercaptoethanol, 1 mM GlutaMax, 1% nonessential amino acid, PS (100 U/ml), and recombinant mouse leukemia inhibitory factor (LIF; 1000 U/ml)]. Transfection was performed using calcium phosphate method or Lipofectamine 3000 reagent.

Neuron induction

Neuron induction from mES cells was followed by an established protocol with modifications (39). Briefly, 2 days before induction, ES cells were seeded on a plate precoated with 0.1% gelatin (Millipore) and Synthemax (1 mg/ml; Corning) without feeder cells and cultured in N2B27 medium (1:1 mix of N2 medium and B27 medium) supplemented with 3 μM GSK3β inhibitor CHIR99021 (Stemgent), 1 μM MEK1/2 inhibitor PD0325901 (Stemgent), and LIF (1000 U/ml). They were then hang-drop cultured in LIF-free ES medium for 2 days to form embryoid bodies (EBs). EBs were transferred to ultralow attachment plate (Corning) and cultivated in LIF-free ES medium for 2 days, followed by N2B27 medium with 5 μM retinoic acid (RA) for 2 days. To induce neuron differentiation, EBs were dissociated by Accutase (Millipore), and the dissociated cells were seeded on a plate precoated with laminin (5 μg/ml) and poly-D-lysine (40 μg/ml) and cultured in N2B27 medium with 5 μM RA.

For neuron induction from NPC, the neocortex was dissected from E13.5 C57BL/6J mouse and incubated with Accutase solution (Millipore) for 15 min at 37°C. The dissociated cells were seeded on ultralow attachment plate for suspension culture at a density of 100,000 cells/ml in culture medium composed of DMEM/F12 (Invitrogen), N2 supplement (Invitrogen), 1% PSA (penicillin-streptomycin-amphotericin; Invitrogen), epidermal growth factor (20 ng/ml; Millipore), and fibroblast growth factor (20 ng/ml; BD Biosciences). To induce neuron differentiation, the suspended NPC aggregates were dissociated by Accutase, and cells were seeded on a plate precoated with poly-D-lysine (40 mg/ml) and cultured in N2B27 medium.

In situ hybridization

Whole embryos were perfused with 4% phosphate-buffered paraformaldehyde (PFA), washed with phosphate-buffered saline (PBS), and cryo-protected with 30% sucrose in PBS. They were then embedded in Tissue-Tec optimal cutting temperature (OCT) (Sakura Finite) and sectioned at 20 μm on a Cryostat (Leica). Sections were secondarily fixed with 4% PFA, treated with acetic anhydride, and dehydrated in a series of ethanol baths. Sense and antisense RNA probes for *Usp11* were labeled using a Digoxigenin (DIG)–RNA labeling kit (Roche). Hybridization was performed overnight at 55°C. Next, the sections were treated with ribonuclease A (20 mg/ml) at 37°C for 30 min and washed with 0.2× saline sodium citrate (SSC) and then 0.1× SSC at 55°C for 30 min each. DIG-labeled RNA probes were immunodetected with antidigoxigenin conjugated to alkaline phosphatase. The antibody conjugate was visualized with chemiluminescent substrates Disodium 3-(4-methoxyspiro {1,2-dioxetane-3,2′-(5′-chloro) tricyclo [3.3.1.13,7]decan}-4-yl)phenyl phosphate (CSPD). Then, the sections were dehydrated in a series of alcohol and xylene, air-dried, and mounted.

Immunoprecipitation and Western blotting

Immunoprecipitation and Western blotting using cell lysates containing equal amounts of proteins were performed as described previously (20).

Mouse husbandry

Mice were housed in a specific pathogen–free animal facility under temperature-controlled (22° ± 2°C) and humidity-controlled (55 ± 5%) conditions with a 12-hour light/12-hour dark circadian cycle and access to food and water. When mice were mated, the morning that vaginal plug was identified was designated as E0.5. During behavioral testing, mice were group-housed with two to five animals of the same sex per cage. All mouse experiments were conducted with approval from the Institutional Animal Care and Use Committee, Academia Sinica, and followed the guidelines of ethical regulations.

Behavioral analyses

All assays were conducted during 1:00 p.m. to 6:00 p.m. light phase by observers who did not know the genotype of the mice until the test had been completed and were performed with 3- to 4-month-old male littermates. For MWM test, mice were trained in a circular pool with a diameter of 1.54 m, filled with milky water and maintained at 20°C. A circular platform (13 cm in diameter and 12.5 cm in height) was placed in the center of one quadrant (target quadrant) and hidden 1 cm beneath the water surface. Training for the hidden platform consisted of four trials each day for four consecutive days. During this period, mice were randomly released to three nontarget quadrants and were allowed to stand on the platform for 15 s before being transferred back to cages. The probe trial was performed on the 5th day in the MWM without a platform. The percentage of time spent by the mouse in each quadrant was recorded. Last, the visible platform, which was marked by a flag, was placed to ensure the swimming ability and visual acuity of the mice. For all of the trials, the maximal swimming duration was 1 min, and the intertrial interval was 15 min. The trajectories of the mice

were recorded and analyzed using TrackMot (Singa Technology Corporation, Taiwan).

For the CFC test, a chamber with an electrified floor grid and a video camera (CleverSys FreezeScan) was used to measure the freezing response. Mice were placed in the chamber, and a 2-s, 0.5-mA foot shock was given every 2 min for four times. The mice were placed back into their cages 2 min after the final shock. Extinction trials were performed at 24 hours later in the same chamber. Each trial duration was 6 min, and the percentage of freezing was analyzed.

For the open field test, mice were individually placed in the apparatus consisting of four transparent Plexiglas arenas (480 mm by 480 mm by 350 mm) in which the floor and walls were covered with black paper to prevent any interference from movements of the neighboring mouse. Each mouse was released into a corner of the box and allowed to explore for 30 min. Mouse behaviors were recorded and analyzed using the ANY-maze software.

For the EPM test, a maze consisting of two open arms (30 cm by 5 cm) with a 1-cm (in height) ledge and two enclosed arms with 15-cm (in height) walls was elevated to a height of 50 cm above the floor. Mice were placed in the central area of the maze, facing one of the open arms. Mouse behaviors were recorded in a 5-min testing period and analyzed using the ANY-maze software.

For the NOR test, mice were individually habituated in a 48 cm by 48 cm by 35 cm open field for 5 min and then tested individually with two identical objects placed in the field. Each mouse was allowed to explore for 10 min with the objects present. After 24 hours, the mouse was tested in the object novelty recognition in which a novel object was replaced with one of the familiar objects. Mouse behaviors were video-recorded and analyzed using the ANY-maze software. Contact is defined by touching the object or staying within 0.5 cm of the object.

For the rotarod test, mice were pretrained twice a day for four consecutive days. For the pretrained trial, the mice were habituated to stay on the rod at a constant speed of 4 rpm for 60 s. On the day of testing, mice were kept in their home cages and acclimated to the testing room for at least 2 hours. For the testing phase, mice were placed on the accelerating rod with the speed from 4 to 40 rpm over a 300-s period for three test trials with 15-min intertrial intervals. The latency to fall of each mouse was recorded. Rotarod data were collected by averaging three trials.

Generation of the *Usp11*-floxed mice

The two loxp sequences were inserted into introns 1 and 9 of the *Usp11* gene using CRISPR-Cas9 to generate the conditional allele. The guide RNA (gRNA) sequences used were 5′-CCGCGATACTA-ACGCCCCCA and 5′-TCTTAGAGTTAACCCCACTT. A T7 promoter sequence (5′-TTAATACGACTCACTATA) was added upstream of gRNA sequences, and a partial tracrRNA sequence (5′-GTTTTA GAGCTAGAAATAGC) was added downstream of the gRNA sequence. The oligo was annealed with a reverse tracrRNA (5′-TTTA-AAAGCACCGACTCGGTGCCACTTTTTCAAGTTGATAACG-GACTAGCCTTATTTTAACTTGCTATTTCTAGCTCTAAAAC) and PCR-amplified using Phusion DNA polymerase (Thermo Fisher Scientific). The amplified product was purified using the QIAquick PCR purification Kit (QIAGEN) and used for in vitro transcription to generate single-guide RNA (sgRNA) with the HiScribe T7 Quick High-Yield RNA Synthesis Kit (NEB). Cas9 mRNA was synthesized using the mMESSAGE mMACHINE T7 ULTRA Kit (Thermo Fisher Scientific), purified using the MEGAclear Transcription Clean-up

Kit (Thermo Fisher Scientific), and eluted with injection buffer [10 mM tris-HCl (pH 7.2) and 0.1 mM EDTA (pH 8.0)]. The quality and quantity of RNAs were analyzed using NanoDrop ND-1000 (Thermo Fisher Scientific). The 5′ and 3′ single-stranded homology directed repair (HDR) templates [5′ single-strand oligodeoxynucleotide (ssODN): 5′-gatgaacagtggcgccaaatcgggaatgggcgagagcgtccactgc-gagctggcgaaagctggtgaggctgggcttcaatgaagccttggccaaggggatcttggA-TAACTTCGTATAGCATACATTATACGAAGTTAT<u>CTC-GAG</u>gggcgttagtatcgcggggtacttagaaatcaaattctgaggatgaagcggtgcg and 3′ ssODN: 5′-caaccccaggtattgcactacatctgtccccatacctatcttagagt-taacccca<u>CTCGAG</u>ATAACTTCGTATAGCATACATTATAC-GAAGTTATcttag<u>a</u>ctcccgtcctacattcaaaatgccagctctgacagggaacat-gggttccagacagacctagctgtaaccctgccactaggcttcaacagtgtcctttac] containing loxp sequence (uppercase) and Xho I site (uppercase and underlined) were synthesized by IDT (Integrated DNA Technologies). Mutations of C to T and G to A were made in the 5′-ssODN and 3′-ssODN (lowercase and underlined), respectively, to disrupt the protospacer adjacent motif (PAM) sequence of gRNA.

For mice production, 3- to 4-week-old C57BL/6J female mice were superovulated with 3.75 to 5 international unit (i.u.) of Pregnant Mare Serum Gonadotrophin (PMSG) (Sigma-Aldrich) followed by 3.75 to 5 i.u. of human chorionic gonadotropin (Sigma-Aldrich) at 46 hours later. The mice were set mating to male mice, and one-cell stage zygotes were collected on the next day. The mixture of Cas9 mRNA, sgRNAs, and ssODNs at the concentration of 50, 50 and 100 ng/μl was injected into both pronuclei and cytoplasm of the zygotes. Injected zygotes were transferred into the oviduct of 0.5-days post coitum (dpc) pseudopregnant ICR female mice. To validate the 5′- and 3′-loxp knock-in, the following primer pairs were used to amplify the region comprising 5′- and 3′-loxp: intron 1 Fw 5′-TCCTATCTTCAGTTGCGTCGG and Rv 5′-CCCCATTTTGTCCT-TAGGCG; intron 9 Fw 5′-GTCATTCCTCCTGGATGGGC and Rv 5′-TGGGACACTGAGGTAGCAGA. The PCR product was digested with Xho I and was further sequenced to confirm that the two loxp sites are intact.

EdU administration

Mice were intraperitoneally injected with EdU at 100 μg/g body weight. Incorporated EdU was detected with the Click-iT EdU Kit (Roche).

Calculation of cell cycle length with EdU-BrdU double labeling

Cell cycle length analysis essentially followed a previously described method (*23*). Briefly, the pregnant female mice were injected intraperitoneally with EdU at a dose of 100 μg/g body weight. Then, the same dose of BrdU was injected at 1.5 hours later. Mice were euthanized at 2 hours after the first injection. Embryos were fixed, frozen-sectioned, and processed for detection of incorporated EdU using the Click-iT Imaging Kit (Invitrogen) and BrdU by anti-BrdU antibodies (MoBu-1, Abcam, ab8039). The section was costained with 4′,6-diamidino-2-phenylindole (DAPI). The cell cycle lengths (Tc) were calculated by the following equation, which is based on the assumptions that all cells in the ventricular zone are proliferating and that the length ratio of each cell cycle is equal to the ratio of the number of cells

$$Tc~(h) = P~cells \times Ti~(time~between~injections = 1.5~hours)/L~cells$$

P cells represent the total number of proliferating cells in the ventricular zone, whereas L cells (leaving fraction) are the number of cells labeled with EdU, but not BrdU.

Terminal deoxynucleotidyl transferase–mediated deoxyuridine triphosphate nick end labeling assay

Apoptotic cells in the sections of embryonic brains were labeled with the In Situ Cell Death Detection Kit Fluorescein (Roche, Basel, Switzerland).

Immunofluorescence

Frozen sections were washed twice with filtered PBS and permeabilized with cytoskeleton (CSK) buffer containing 50 mM NaCl, 3 mM MgCl$_2$, 300 mM sucrose, 0.5% Triton X-100, and 10 mM Pipes (pH 6.8) for 20 min and blocked with PBS supplemented with 10% goat serum and 1% bovine serum albumin for 1 hour. Cells were incubated with primary antibody at 4°C overnight. The slides were washed three times with 1% PBS at room temperature and then incubated with FITC-conjugated secondary antibody (Invitrogen) together with DAPI (1 µg/ml) for 1 hour.

Microscopy and image analysis

Macro-view of stained sections was examined by an Olympus SZX16 Stereo microscope equipped with a 1× objective lens (Olympus), and fluorescent images were captured by a DP80 digital camera with controller software (Analysis LS Research; Olympus). For microview, the sections were examined by a Leica SP5 Confocal Microscope equipped with a 40× or 60× objective lens (Leica), and images were captured by a cooled charge-coupled device camera operated by the Leica Application Suite Advanced Fluorescence Software. Fluorescence intensity was quantified by the ImageJ software. For quantifying cells in a brain section, an appropriate image width was chosen (IUE experiment: 300 µm; terminal deoxynucleotidyl transferase–mediated deoxyuridine triphosphate nick end labeling assay: 1600 µm for E18.5 and 800 µm for E12.5 to E15.5; all other experiments: 1000 µm for P7, 450 µm for E18.5, and 350 µm for E11.5 to E15.5), and the numbers or distribution of labeled cells in the entire cortical column were quantified.

RNA extraction, RT-PCR, and real-time PCR

Total RNA was extracted using Trizol reagent (Invitrogen). One microgram of total RNA was used for cDNA synthesis with the iScript reverse transcriptase (Bio-Rad). Real-time PCR was performed using the Power SYBR Green PCR Master Kit (Applied Biosystems) on a LightCycler 480 (Roche). The conditions for PCR analysis were 95°C for 15 min, 35 cycles at 94°C for 15 s, 55°C for 30 s, and 70°C for 30 s. Expression data were normalized to the mean of housekeeping gene glyceraldehyde-3-phosphate dehydrogenase. The primer sequences are as follows: Usp11: Fw 5′-AACAACAT-ACCGGACGAGGAT, Rv 5′-CCTTCATGCCTAGAGGGTTCC; Sox11: Fw 5′-CGACGACCTCATGTTCGACC, Rv 5′-GACAGG-GATAGGTTCCCCG; Pax6: Fw 5′-TGGCAAACAACCTGCCTATG, Rv 5′-TGCACGAGTATGAGGAGGTCT; Tuj1: Fw 5′-TAGAC-CCCAGCGGCAACTAT, Rv 5′-GTTCCAGGTTCCAAGTC-CACC; Gapdh: Fw 5′-AGGTCGGTGTGAACGGATTT, Rv 5′-TG-TAGACCATGTAGTTGAGGTCA.

RNA interference

Lentivirus-based shRNA constructs were obtained from National RNAi Core Facility in Taiwan. Lentivirus generation and transduction were described previously (40). The target sequences of various shRNAs are as follows: shUSP11#1: 5′-GCAGAACCATAAACGACGAAA; shUsp11#2: 5′-CCAGACCTCTACAAATATGAT; and shUsp11#3: 5′-CCTACTATGGTCTGATACTTT.

Deubiquitination assays

For in vitro deubiquitination, ubiquitinated Sox11 was purified from 293T cells transfected with Sox11-Flag and His-ubiquitin by M2 agarose beads (Sigma-Aldrich) and then eluted by Flag peptide. Myc-Usp11 or its mutant was affinity-purified with c-Myc agarose beads from transfected 293T cells and incubated with ubiquitinated Sox11 in 40-µl deubiquitination reaction mix containing 100 mM Hepes (pH 7.4), 500 mM NaCl, 100 mM MgCl$_2$, 100 mM dithiothreitol, and 10 mM adenosine 5′-triphosphate at 37°C for 2 hours. Reaction products were analyzed by Western blot.

For in vivo deubiquitination, cells transfected with various constructs together with Sox11-Flag and His-ubiquitin were treated with 1 µM MG132 for 16 hours and then lysed with radioimmuno-precipitation assay lysis buffer containing 50 mM tris (pH 8.0), 0.15 M NaCl, 1% NP-40, 1% sodium deoxycholate, 0.1% SDS, 1 mM phenylmethylsulfonyl fluoride (PMSF), aprotinin (1 µg/ml), and leupeptin (1 µg/ml). Lysates were used for immunoprecipitation with anti-Flag antibody, followed by Western blot with anti-His antibody. Alternatively, cells were lysed under denaturing conditions by buffer A [6 M guanidine-HCl, 0.1 M Na$_2$HPO$_4$/NaH$_2$PO$_4$ (pH 8.0), and 10 mM imidazole], and lysates were incubated with nickel-nitrilotriacetic acid (Ni-NTA) agarose for 2 hours at 4°C. The beads were washed twice with buffer A/TI {1 vol buffer A:3 vol buffer TI [25 mM tris-HCl (pH 6.8) and 20 mM imidazole]} and five times with buffer TI and then analyzed by Western blot. In all experiments, equal expression of His-ubiquitin was verified by Western blot.

Luciferase reporter assay

Cells were cotransfected with pGL3-based reporter construct and pCMV-Renilla. Forty hours after transfection, luciferase activity in cell lysate was assayed by the Dual Luciferase Reporter Assay System (Promega). The relative promoter activity was expressed as fold changes in firefly luciferase activity after normalization to the Renilla luciferase activity.

In utero electroporation

E12.5, E13.5, or E15.5 embryos were visualized through the uterus using a fiber-optic light source. DNA solution containing cDNA (1 µg/µl) and/or shRNA expression constructs together with CAG-mCherry plasmid (0.2 µg/µl) and 1% fast green (Sigma-Aldrich) was injected with a glass capillary into the ventricle of each embryo, and electroporation was performed with a CUY21 Electroporator (Nepa Gene) in a series of five square-wave current pulses (35 V, 100 ms × 5). Embryos were allowed to develop until E15.5 or E18.5 and were analyzed by direct visualization of the mCherry expression.

Sample preparation for ubiquitylome or proteome analyses

Cells treated with 5 µM MG132 for 1 hour or cortices dissected from E17.5 mouse embryos were lysed in buffer containing 8 M urea, 50 mM tris-HCl (pH 8.0), 150 mM NaCl, 1 mM EDTA, aprotinin (2 µg/ml), leupeptin (10 µg/ml), and 1 mM PMSF. Lysates were reduced with 5 mM dithiothreitol (Sigma-Aldrich) at 37°C for 45 min followed by alkylation with 10 mM iodoacetamide (Sigma-Aldrich) for 30 min at room temperature in the dark. Lysates were diluted to 4 M urea with 50 mM tris-HCl (pH 8.0) and digested with Lys-C (WAKO) for 4 hours at 37°C. The peptide mixture was further diluted to 2 M urea and digested with trypsin (Promega) overnight at 37°C. The resulting peptides were acidified with fluoroacetic acid,

desalted using a tC18 sep-Pak SPE cartridge or C18 Zip-Tip, and lyophilized.

Quantitative ubiquitylome analysis using TMT labeling and LC-MS/MS

For K-ε-GG peptide enrichment, lyophilized peptides were resuspended in immunoaffinity purification (IAP) buffer (Cell Signaling Technology) and incubated with PTMScan Ubiquitin Remnant Motif (K-ε-GG) Antibody Bead Conjugate (Cell Signaling Technology) overnight at 4°C. The beads were washed twice with ice-cold IAP buffer, followed by washing three times with ice cold water. Ubiquitinated peptides were eluted with 80 μl of 0.15% trifluoroacetic acid twice. The eluent was cleaned up by C18 Stage Tips (Millipore) and then lyophilized.

For TMT labeling, peptides before and after K-ε-GG peptide enrichment were reconstituted in 100 mM triethyl ammonium bicarbonate and incubated with TMT-labeling reagent (0.8 mg TMT-129 or TMT-131 in 41 μl of anhydrous acetonitrile) for 1 hour at room temperature. The reaction was quenched by adding 8 μl of 4% hydroxylamine. The solution was cleaned up with C18 Zip-Tip and lyophilized.

After TMT labeling, peptides for proteome analysis were fractionated by strong cation exchange (SCX) chromatography. Briefly, peptides were resuspended in SCX buffer A [7 mM KH_2PO_4 (pH 2.65) and 30% acetonitrile] and separated on a PolySULFOETHYL A column (200 × 4.6 mm, 5 μm, 200 Å) using an Agilent 1100 system. A 160-min SCX gradient was used for separation at a flow rate of 1 ml/min. The gradient consisted of a 20-min equilibration phase with 100% buffer A, a linear increase to 20% buffer B [7 mM KH_2PO_4 (pH 2.65), 350 mM KCl, and 30% acetonitrile] within 20 min, a second linear increase to 50% buffer B in 40 min, a third linear increase to 75% buffer B in 10 min, and 100% buffer B for 10 min.

NanoLC-MS/MS analysis was performed on a Thermo Fisher Scientific UltiMate 3000 RSLCnano system connected to a Thermo Orbitrap Fusion mass spectrometer (Thermo Fisher Scientific, Bremen, Germany) equipped with a PicoView nanospray interface (New Objective, Woburn, MA). Peptide mixtures were loaded onto a 75-μm-inner diameter (ID), 25-cm-long Acclaim PepMap Rapid Separation Liquid Chromatography (RSLC) packed with 2-μm particles with a pore width of 100 Å and were separated using a segmented gradient in 150 min from 5 to 40% solvent B (acetonitrile with 0.1% formic acid) at a flow rate of 300 nl/min and a column temperature of 40°C. Solvent A was 0.1% formic acid in water. The mass spectrometer was operated in the data-dependent mode. Briefly, survey scans of peptide precursors from 350 to 1600 m/z were performed at 120K resolution with a 2×10^5 ion count target. Tandem MS was performed by isolation window at 2 Da with the quadrupole, higher-energy collisional dissociation (HCD) fragmentation with a normalized collision energy of 38, and scan MS analysis in the Orbitrap. The minimum MS signal for triggering MS/MS was set to 50,000. The MS^2 ion count target was set to 10^5, and the maximum injection time was 200 ms. Only those precursors with charge states 2 to 7 were sampled for MS^2. The instrument was run in top speed mode with 3-s cycles, the dynamic exclusion duration was set to 60 s with a 10 ppm tolerance around the selected precursor and its isotopes, and the monoisotopic precursor selection was turned on.

For MS data analysis, Proteome Discoverer (1.4) software (Thermo Fisher Scientific, San Jose, CA) was used to perform database searching against the Swiss-Prot Mouse database using both the Sequest algorithms with the settings of 10 ppm precursor mass tolerance and 0.02-Da fragment mass tolerance. Trypsin was specified as the digesting enzyme, and two missed cleavages are allowed. Cysteine carbamidomethylation and TMT modifications (N terminus) were defined as fixed modifications and methionine oxidation, and TMT modifications (ubiquitinated lysine and lysine residues) were defined as the variable modifications. The results were filtered by medium and high confident peptides with a global false discovery rate (FDR) < 1% based on a target-decoy approach, and first-ranked peptides were included in the results. For quantification, the ratios of TMT reporter ion intensities in MS/MS spectra [mass/charge ratio (m/z) 129.14 and 131.14] from raw data sets were used to calculate fold changes between samples via the relative ratio to the reference pool. Only peptides unique for a given protein were considered for quantitation.

Label-free quantitative LC-MS/MS analysis

NanoLC−nanoESi-MS/MS analysis was performed on a Thermo UltiMate 3000 RSLCnano System connected to an Thermo Orbitrap Fusion mass spectrometer (Thermo Fisher Scientific, Bremen, Germany) equipped with a nanospray interface (New Objective, Woburn, MA) and followed procedures as previously described (41). Briefly, peptide mixtures were loaded onto a 75-μm-ID, 25-cm-long PepMap C18 column (Thermo Fisher Scientific) packed with 2-μm particles with a pore width of 100 Å and were separated using a segmented gradient in 120 min from 5 to 35% solvent B (0.1% formic acid in acetonitrile) at a flow rate of 300 nl/min. Solvent A was 0.1% formic acid in water. The mass spectrometer was operated in the data-dependent mode. Briefly, survey scans of peptide precursors from 350 to 1600 m/z were performed at 240K resolution with a 2×10^5 ion count target. Tandem MS was performed by isolation window at 1.6 Da with the quadrupole, HCD fragmentation with a normalized collision energy of 30, and rapid scan MS analysis in the ion trap. The MS^2 ion count target was set to 1×10^4, and the maximum injection time was 50 ms. Only those precursors with charge states 2 to 6 were sampled for MS^2. The instrument was run in top speed mode with 3-s cycles, the dynamic exclusion duration was set to 15 s with a 10 ppm tolerance around the selected precursor and its isotopes, and monoisotopic precursor selection was turned on.

Label-free quantification was processed using the Progenesis QI for proteomics 4.1 (Nonlinear Dynamics Ltd., Newcastle, UK) with the default peak-picking settings. "Relative quantitation using nonconflicting peptides" setting was used, which calculates protein abundance in a run as the sum of all the unique peptide ion abundances corresponding to that protein. Peptide identification was performed using Mascot search engine (v.2.7.0; Matrix Science, Boston, MA, USA) against the Swiss-Prot Mouse database (17,046 entries total). Search criteria used were trypsin digestion, allowing up to two missed cleavages, mass accuracy of 10 ppm for the parent ion, and 0.6 Da for the fragment ions. Fixed modifications were set as carbamidomethyl (cysteine), and variable modifications were set as oxidation (methionine) and acetylation (protein N terminus). A decoy database search was performed, and identified peptides were filtered with 1% FDR. The resulting quantifications are median-normalized for each group, and statistics was determined by one-way ANOVA with Tukey's post hoc test with a threshold of $P < 0.05$.

Bioinformatics

GO analysis was carried out using the online bioinformatics tool DAVID v6.8 (https://david.ncifcrf.gov/), and GO terms were filtered by P value <0.05.

Statistical analysis

Statistical analysis was performed using two-tailed Student's *t* tests for comparisons between two groups and one-way analysis of variance (ANOVA) with Tukey's post hoc test for multigroup comparisons.

SUPPLEMENTARY MATERIALS

Supplementary material for this article is available at http://advances.sciencemag.org/cgi/content/full/7/7/eabc6093/DC1

View/request a protocol for this paper from *Bio-protocol*.

REFERENCES AND NOTES

1. M. Florio, W. B. Huttner, Neural progenitors, neurogenesis and the evolution of the neocortex. *Development* **141**, 2182–2194 (2014).
2. R. S. Desikan, A. J. Barkovich, Malformations of cortical development. *Ann. Neurol.* **80**, 797–810 (2016).
3. R. Guerrini, W. B. Dobyns, Malformations of cortical development: Clinical features and genetic causes. *Lancet Neurol.* **13**, 710–726 (2014).
4. A. S. Nord, K. Pattabiraman, A. Visel, J. L. R. Rubenstein, Genomic perspectives of transcriptional regulation in forebrain development. *Neuron* **85**, 27–47 (2015).
5. K. J. Yoon, C. Vissers, G. L. Ming, H. Song, Epigenetics and epitranscriptomics in temporal patterning of cortical neural progenitor competence. *J. Cell Biol.* **217**, 1901–1914 (2018).
6. K. J. Yoon, B. K. Koo, S. K. Im, H. W. Jeong, J. Ghim, M. C. Kwon, J. S. Moon, T. Miyata, Y. Y. Kong, Mind bomb 1-expressing intermediate progenitors generate notch signaling to maintain radial glial cells. *Neuron* **58**, 519–531 (2008).
7. X. Zhao, D. D'Arca, W. K. Lim, M. Brahmachary, M. S. Carro, T. Ludwig, C. C. Cardo, F. Guillemot, K. Aldape, A. Califano, A. Iavarone, A. Lasorella, The N-Myc-DLL3 cascade is suppressed by the ubiquitin ligase Huwe1 to inhibit proliferation and promote neurogenesis in the developing brain. *Dev. Cell* **17**, 210–221 (2009).
8. T. C. Tuoc, A. Stoykova, Trim11 modulates the function of neurogenic transcription factor Pax6 through ubiquitin-proteosome system. *Genes Dev.* **22**, 1972–1986 (2008).
9. C. C. Homan, R. Kumar, L. S. Nguyen, E. Haan, F. L. Raymond, F. Abidi, M. Raynaud, C. E. Schwartz, S. A. Wood, J. Gecz, L. A. Jolly, Mutations in USP9X are associated with X-linked intellectual disability and disrupt neuronal cell migration and growth. *Am. J. Hum. Genet.* **94**, 470–478 (2014).
10. Z. Huang, Q. Wu, O. A. Guryanova, L. Cheng, W. Shou, J. N. Rich, S. Bao, Deubiquitylase HAUSP stabilizes REST and promotes maintenance of neural progenitor cells. *Nat. Cell Biol.* **13**, 142–152 (2011).
11. M. Sakurai, K. Ayukawa, R. Setsuie, K. Nishikawa, Y. Hara, H. Ohashi, M. Nishimoto, T. Abe, Y. Kudo, M. Sekiguchi, Y. Sato, S. Aoki, M. Noda, K. Wada, Ubiquitin C-terminal hydrolase L1 regulates the morphology of neural progenitor cells and modulates their differentiation. *J. Cell Sci.* **119**, 162–171 (2006).
12. S. Reiprich, M. Wegner, From CNS stem cells to neurons and glia: Sox for everyone. *Cell Tissue Res.* **359**, 111–124 (2015).
13. P. Bhattaram, A. Penzo-Méndez, E. Sock, C. Colmenares, K. J. Kaneko, A. Vassilev, M. L. Depamphilis, M. Wegner, V. Lefebvre, Organogenesis relies on SoxC transcription factors for the survival of neural and mesenchymal progenitors. *Nat. Commun.* **1**, 9 (2010).
14. M. Bergsland, D. Ramskold, C. Zaouter, S. Klum, R. Sandberg, J. Muhr, Sequentially acting Sox transcription factors in neural lineage development. *Genes Dev.* **25**, 2453–2464 (2011).
15. L. Mu, L. Berti, G. Masserdotti, M. Covic, T. M. Michaelidis, K. Doberauer, K. Merz, F. Rehfeld, A. Haslinger, M. Wegner, E. Sock, V. Lefebvre, S. Couillard-Despres, L. Aigner, B. Berninger, D. C. Lie, SoxC transcription factors are required for neuronal differentiation in adult hippocampal neurogenesis. *J. Neurosci.* **32**, 3067–3080 (2012).
16. C. Chen, G. A. Lee, A. Pourmorady, E. Sock, M. J. Donoghue, Orchestration of neuronal differentiation and progenitor pool expansion in the developing cortex by SoxC genes. *J. Neurosci.* **35**, 10629–10642 (2015).
17. Y. Hoshiba, T. Toda, H. Ebisu, M. Wakimoto, S. Yanagi, H. Kawasaki, Sox11 balances dendritic morphogenesis with neuronal migration in the developing cerebral cortex. *J. Neurosci.* **36**, 5775–5784 (2016).
18. M. Bergsland, M. Werme, M. Malewicz, T. Perlmann, J. Muhr, The establishment of neuronal properties is controlled by Sox4 and Sox11. *Genes Dev.* **20**, 3475–3486 (2006).
19. B. Muralidharan, Z. Khatri, U. Maheshwari, R. Gupta, B. Roy, S. J. Pradhan, K. Karmodiya, H. Padmanabhan, A. S. Shetty, C. Balaji, U. Kolthur-Seetharam, J. D. Macklis, S. Galande, S. Tole, LHX2 interacts with the NuRD complex and regulates cortical neuron subtype determinants Fezf2 and Sox11. *J. Neurosci.* **37**, 194–203 (2017).
20. H. C. Wu, Y. C. Lin, C. H. Liu, H. C. Chung, Y. T. Wang, Y. W. Lin, H. I. Ma, P. H. Tu, S. E. Lawler, R. H. Chen, USP11 regulates PML stability to control Notch-induced malignancy in brain tumours. *Nat. Commun.* **5**, 3214 (2014).

21. E. Karaca, T. Harel, D. Pehlivan, S. N. Jhangiani, T. Gambin, Z. Coban Akdemir, C. Gonzaga-Jauregui, S. Erdin, Y. Bayram, I. M. Campbell, J. V. Hunter, M. M. Atik, H. Van Esch, B. Yuan, W. Wiszniewski, S. Isikay, G. Yesil, O. O. Yuregir, S. Tug Bozdogan, H. Aslan, H. Aydin, T. Tos, A. Aksoy, D. C. De Vivo, P. Jain, B. B. Geckinli, O. Sezer, D. Gul, B. Durmaz, O. Cogulu, F. Ozkinay, V. Topcu, S. Candan, A. H. Cebi, M. Ikbal, E. Yilmaz Gulec, A. Gezdirici, E. Koparir, F. Ekici, S. Coskun, S. Cicek, K. Karaer, A. Koparir, M. B. Duz, E. Kirat, E. Fenercioglu, H. Ulucan, M. Seven, T. Guran, N. Elcioglu, M. S. Yildirim, D. Aktas, M. Alikasifoglu, M. Ture, T. Yakut, J. D. Overton, A. Yuksel, M. Ozen, D. M. Muzny, D. R. Adams, E. Boerwinkle, W. K. Chung, R. A. Gibbs, J. R. Lupski, Genes that affect brain structure and function identified by rare variant analyses of mendelian neurologic disease. *Neuron* **88**, 499–513 (2015).
22. B. J. Molyneaux, P. Arlotta, J. R. Menezes, J. D. Macklis, Neuronal subtype specification in the cerebral cortex. *Nat. Rev. Neurosci.* **8**, 427–437 (2007).
23. B. Martynoga, H. Morrison, D. J. Price, J. O. Mason, Foxg1 is required for specification of ventral telencephalon and region-specific regulation of dorsal telencephalic precursor proliferation and apoptosis. *Dev. Biol.* **283**, 113–127 (2005).
24. J. A. Gorski, T. Talley, M. Qiu, L. Puelles, J. L. Rubenstein, K. R. Jones, Cortical excitatory neurons and glia, but not GABAergic neurons, are produced in the Emx1-expressing lineage. *J. Neurosci.* **22**, 6309–6314 (2002).
25. S. Goebbels, I. Bormuth, U. Bode, O. Hermanson, M. H. Schwab, K. A. Nave, Genetic targeting of principal neurons in neocortex and hippocampus of NEX-Cre mice. *Genesis* **44**, 611–621 (2006).
26. T. Kawauchi, Cellular insights into cerebral cortical development: Focusing on the locomotion mode of neuronal migration. *Front. Cell. Neurosci.* **9**, 394 (2015).
27. N. D. Udeshi, P. Mertins, T. Svinkina, S. A. Carr, Large-scale identification of ubiquitination sites by mass spectrometry. *Nat. Protoc.* **8**, 1950–1960 (2013).
28. G. C. McAlister, E. L. Huttlin, W. Haas, L. Ting, M. P. Jedrychowski, J. C. Rogers, K. Kuhn, I. Pike, R. A. Grothe, J. D. Blethrow, S. P. Gygi, Increasing the multiplexing capacity of TMTs using reporter ion isotopologues with isobaric masses. *Anal. Chem.* **84**, 7469–7478 (2012).
29. A. Spiliotopoulos, L. Blokpoel Ferreras, R. M. Densham, S. G. Caulton, B. C. Maddison, J. R. Morris, J. E. Dixon, K. C. Gough, I. Dreveny, Discovery of peptide ligands targeting a specific ubiquitin-like domain-binding site in the deubiquitinase USP11. *J. Biol. Chem.* **294**, 424–436 (2019).
30. R. Song, X. Ling, M. Peng, Z. Xue, J. Cang, F. Fang, Maternal sevoflurane exposure causes abnormal development of fetal prefrontal cortex and induces cognitive dysfunction in offspring. *Stem Cells Int.* **2017**, 6158468 (2017).
31. S. Fazel Darbandi, S. E. Robinson Schwartz, Q. Qi, R. Catta-Preta, E. L. Pai, J. D. Mandell, A. Everitt, A. Rubin, R. A. Krasnoff, S. Katzman, D. Tastad, A. S. Nord, A. J. Willsey, B. Chen, M. W. State, V. S. Sohal, J. L. R. Rubenstein, Neonatal Tbr1 dosage controls cortical layer 6 connectivity. *Neuron* **100**, 831–845.e7 (2018).
32. S. J. Sanders, X. He, A. J. Willsey, A. G. Ercan-Sencicek, K. E. Samocha, A. E. Cicek, M. T. Murtha, V. H. Bal, S. L. Bishop, S. Dong, A. P. Goldberg, C. Jinlu, J. F. Keaney III, L. Klei, J. D. Mandell, D. Moreno-De-Luca, C. S. Poultney, E. B. Robinson, L. Smith, T. Solli-Nowlan, M. Y. Su, N. A. Teran, M. F. Walker, D. M. Werling, A. L. Beaudet, R. M. Cantor, E. Fombonne, D. H. Geschwind, D. E. Grice, C. Lord, J. K. Lowe, S. M. Mane, D. M. Martin, E. M. Morrow, M. E. Talkowski, J. S. Sutcliffe, C. A. Walsh, T. W. Yu, C. Autism Sequencing, D. H. Ledbetter, C. L. Martin, E. H. Cook, J. D. Buxbaum, M. J. Daly, B. Devlin, K. Roeder, M. W. State, Insights into autism spectrum disorder genomic architecture and biology from 71 risk loci. *Neuron* **87**, 1215–1233 (2015).
33. N. Bogershausen, B. Wollnik, Mutational landscapes and phenotypic spectrum of SWI/SNF-related intellectual disability disorders. *Front. Mol. Neurosci.* **11**, 252 (2018).
34. T. Regad, C. Bellodi, P. Nicotera, P. Salomoni, The tumor suppressor Pml regulates cell fate in the developing neocortex. *Nat. Neurosci.* **12**, 132–140 (2009).
35. A. Kavyanifar, S. Turan, D. C. Lie, SoxC transcription factors: Multifunctional regulators of neurodevelopment. *Cell Tissue Res.* **371**, 91–103 (2018).
36. S. Shim, K. Y. Kwan, M. Li, V. Lefebvre, N. Sestan, Cis-regulatory control of corticospinal system development and evolution. *Nature* **486**, 74–79 (2012).
37. A. Hempel, A. T. Pagnamenta, M. Blyth, S. Mansour, V. McConnell, I. Kou, S. Ikegawa, Y. Tsurusaki, N. Matsumoto, A. Lo-Castro, G. Plessis, B. Albrecht, A. Battaglia, J. C. Taylor, M. F. Howard, D. Keays, A. S. Sohal; DDD Collaboration, S. J. Kühl, U. Kini, A. McNeill, Deletions and de novo mutations of SOX11 are associated with a neurodevelopmental disorder with features of Coffin-Siris syndrome. *J. Med. Genet.* **53**, 152–162 (2016).
38. Y. Tsurusaki, E. Koshimizu, H. Ohashi, S. Phadke, I. Kou, T. Shiina, T. Suzuki, N. Okamoto, S. Imamura, M. Yamashita, S. Watanabe, K. Yoshiura, H. Kodera, S. Miyatake, M. Nakashima, H. Saitsu, K. Ogata, S. Ikegawa, N. Miyake, N. Matsumoto, De novo SOX11 mutations cause Coffin-Siris syndrome. *Nat. Commun.* **5**, 4011 (2014).
39. Q. L. Ying, A. G. Smith, Defined conditions for neural commitment and differentiation. *Methods Enzymol.* **365**, 327–341 (2003).
40. Y. T. Wang, J. Chen, C. W. Chang, J. Jen, T. Y. Huang, C. M. Chen, R. Shen, S. Y. Liang, I. C. Cheng, S. C. Yang, W. W. Lai, K. H. Cheng, T. S. Hsieh, M. Z. Lai, H. C. Cheng, Y. C. Wang,

R. H. Chen, Ubiquitination of tumor suppressor PML regulates prometastatic and immunosuppressive tumor microenvironment. *J. Clin. Invest.* **127**, 2982–2997 (2017).

41. H. Y. Lee, J. C. Chao, K. Y. Cheng, J. Y. Leu, Misfolding-prone proteins are reversibly sequestered to an Hsp42-associated granule upon chronological aging. *J. Cell Sci.* **131**, jcs220202 (2018).

Citation: S.-Y. Chiang, H.-C. Wu, S.-Y. Lin, H.-Y. Chen, C.-F. Wang, N.-H. Yeh, J.-H. Shih, Y.-S. Huang, H.-C. Kuo, S.-J. Chou, R.-H. Chen, Usp11 controls cortical neurogenesis and neuronal migration through Sox11 stabilization. *Sci. Adv.* **7**, eabc6093 (2021).